Energieforschungsprogramm

Publizierbarer Endbericht

Programmsteuerung:

Klima- und Energiefonds

Programmabwicklung:

Österreichische Forschungsförderungsgesellschaft mbH (FFG)

Endbericht erstellt am 05/12/2022

Projekttitel:

Galion

Projektnummer: 871676

Ausschreibung	5. Ausschreibung Energieforschungsprogramm	
Projektstart	01/03/2019	
Projektende	31/08/2022	
Gesamtprojektdauer	2 Monate	
(in Monaten)	42 Monate	
ProjektnehmerIn	Virtual Vehicle Research GmbH	
(Institution)	Viltual Verlicle Research Offibri	
AnsprechpartnerIn	Christiane Essl	
Postadresse	Inffeldgasse 21a, 8010 Graz	
Telefon	+43 316 873 9001	
Fax	+43 316 873 9002	
E-mail	info@v2c2.at	
Website	www.v2c2.at	

Galion

GAssensorik für Li-IONen Batteriesysteme

AutorInnen:

Michael Rabe, Helmut Krasa, Daniel Bautista Anguís, Florian Maxl, Michael Donnelly, Gabriel Ferdigg, Christiane Essl

Inhaltsverzeichnis 1

1	Inhaltsve	rzeichnis	4
2	Introduct	ion	5
3	Content	presentation	6
3	3.1 Sen	sor selection	6
	3.1.1	Selection of sufficient sensor technologies	6
	3.1.2	Benchmark of sensors for the first adoption of sensor platform	7
3	3.2 Dev	elopment of a functional polymer	8
	3.2.1	Generation 1	9
	3.2.2	Generation 2	16
3	3.3 Ada	ption of sensor technologies	18
	3.3.1	System design	18
	3.3.2	Multi-pixel gas sensor for selective detection of critical battery states	19
	3.3.3	Warning signal algorithm	21
	3.3.4	Onset temperature of the warning signal	23
	3.3.5	Prototype for a battery demonstrator	25
3	3.4 Vali	dation of error detection	25
	3.4.1	Heating setup	25
	3.4.2	Setups to analyze electrolyte advection behavior	26
	3.4.3	Degassing Temperatures of the polymer matrix	29
	3.4.4	Degassing Temperatures of the polymer tracer gases	29
	3.4.5	Long-term stability of the polymers	30
	3.4.6	Diffusion in showcase	36
3	3.5 Vali	dation of the sensors in battery systems	40
	3.5.1	FUSA Concept	41
3	3.6 Buil	ding of sensor platforms	42
	3.6.1	ViF platform containing the following sensors was built:	42
	3.6.2	IES/TUG platform containing the following sensors	43
	3.6.3	Battery test system for Samsung SDI	43
	3.6.4	Update of existing ViF platform	44
	3.6.5	New microcontroller-based sensor platform for battery tests	44
4	Results a	and conclusion	46
5	Outlook a	and recommendations	47
6	Contact	datadata	48

Klima- und Energiefonds des Bundes – Abwicklung durch die Österreichische Forschungsförderungsgesellschaft FFG

2 Introduction

The automotive industry is forcing the manufacturers of Li-ion battery systems to further increase the energy and packing density. For reasons of synergy, the same technology is used new or used (second life) for solar storage, grid stabilization, high-availability emergency power supply and similar applications. It is a major challenge to detect impending errors in such systems to initiate a reduction in performance or maintenance or replacement. The problem is further exacerbated by the possibility of improper repair or manipulation by private individuals. There are types of faults in Li-ion battery systems that are difficult to detect with classic monitoring devices. In particular, the detection of local overheating, leakage of electrolyte vapor from damaged cells, or water condensation in the system (battery systems are often placed outdoors).

A local overtemperature can occur on damaged or overloaded high-current conductors or electronic components. As a result, the excess temperature can lead to insulation damage, short circuits, thermal runaway of a neighboring Li-ion cell, etc. Local excess temperature is not always detected due to the limited number of temperature sensors.

A Li-ion cell damaged mechanically or by internal faults/gas pressure can release electrolyte vapor into the battery system. The flammable electrolyte vapor poses a risk of explosion. The risk is currently only recognized when the drying cell becomes noticeable due to increased internal resistance.

Increased humidity or a leaking cooling system can cause water films and, as a result, corrosion, electrolysis, and short circuits, especially on the circuit boards. Currently, the water film is only recognized by a possibly reduced insulation resistance to ground.

The aim of this project is to develop and test a new complementary battery-monitoring technology based on low-cost gas sensors and functional polymers

- · Selection of sensors for the sensor board
- Development of a functional polymer which releases easily detectable tracergas at overtemperature
- Testing detection of failures in a controlled environment
- Testing detection of failures in realistic environment inside a battery housing
- Measuring the gas concentrations inside battery packs during normal operation

The work is divided into the following main tasks

Validation and selection of low-cost gas sensors for battery applications with usage > 10 years

Klima- und Energiefonds des Bundes – Abwicklung durch die Österreichische Forschungsförderungsgesellschaft FFG

- Development and characterization of a functional polymer for insulation of electric components with the necessary properties (service life, mechanical and electrical properties)
- Development of a false/positive resistive algorithm as the sensor signal output
- · Development of an updated safety concept including functional safety
- Battery pack demonstrator with the developed technologies

The project is running due to the energy research program – 5th announcement, more specifically in the subsection electrochemical storages. The focus is on monitoring and diagnosis concepts for battery systems.

3 Content presentation

3.1 Sensor selection

3.1.1 Selection of sufficient sensor technologies

To facilitate a relatively low-cost sensor platform and at the same time ensure proper detection of the additive (tracer gas) and precursor gases of battery failures, the decision was made to develop two sensor boards. Sensor board 1 includes sensor for a possible series product, which must be small enough to be placed inside a battery pack and contain low-cost sensors, which should be able to detect the precursor gases and possible additives. Sensor board 2 contains more accurate but also more expensive and bulkier sensors, which can give more insight into what is detectable with sensor board 1 and to quantify the results obtained by sensor board 1. A literature review by PCCL revealed that possible tracer gases could include (i) VOCs, (ii) NO_X, or (iii) NH₃. The sensor boards should also be capable of detecting precursor gases such as (i) H₂, (ii) VOCs, (iii) CO₂ and (iv) CO.

Sensor board 1 contains mostly metal oxide (MOX) sensors. This sensor technology is based on the change of conductance (resistivity) upon the surface reaction with oxidizing or reducing gases. To obtain selectivity the sensors are typically coated with vendor specific materials. Cross-sensitivity to other gases is, however, always present. Further, photoacoustic (CO₂), electrochemical (H₂ and CO), as well as a jfet (NH₃) sensor were selected for sensor board 1 (cf. Table 1), together with a priority ranking. As the NH3 T300 sensor from Sensic was not ready for the market at the time, it had to be withdrawn. Similarly, the photoacoustic Sensirion SCD40 sensor could not be used for the series sensor board since the date of market entry was postponed. The series product board, which was produced for the measurements with Samsung SDI contained the remaining sensors.

Table 1: Sensors for sensor board 1 (series product).

VENDOR	MODEL	MEAS. QUANTITY	PRINCIPLE	PRIORITY
Sensirion	SGP30	VOC, H ₂ , Nox, NH3	MOX	1
Sensirion	SCD40	CO ₂	Photoacoustic	3
Figaro	TGS 5141	H ₂ , CO	Electrochemical	3
IDT	SGAS701	H_2	MOX	1
Sensic	NH3-T300	NH ₃	jfet	2
AMS	IAQ-CORE	VOC	MOX	3
SGX Sensortech	MiCS 6814	NH ₃ , NO ₂ , CO	MOX	1
Bosch	BME – 280	RH, p, T	-	2
Sensirion	SHT3x	TH, T	-	2

Table 2 contains sensors which were selected for the reference board. Again, MOX sensors are used. However, also more sophisticated technologies, such as photoionization detector (PID) for VOCs, non-dispersive infrared detector (NDIR) for CO₂ and electrochemical sensors (for NO and NO₂) are used. The DGS-O3 is a MOX sensor which is sensitive to O₃ and NO₂ and is intended to correct possible cross interferences of other sensors.

Table 2: Sensors for sensor board 1 (reference sensor board).

VENDOR	MODEL	MEAS. QUANTITY	PRINCIPLE	PRIORITY
Sensirion	SCD30	CO ₂	NDIR	1
Alphasense	PID-AH2	VOC	PID	1
Alphasense	VOC Sensor	VOC	MOX	1
	p-type Metal			
	Oxide			
Sensirion	SHT31	RH, T	-	1
Alphasense	NO-A4	NO	Electrochemical	1
Alphasense	NO2-A43F	NO ₂	Electrochemical	1
IDT	SGAS701	H ₂	MOX	1
Sensic	NH3-T300	NH ₃	jfet	1
SPEC Sensors	DGS-O3	O ₃	Electrochemical (thin film)	1

3.1.2 Benchmark of sensors for the first adoption of sensor platform

Four custom variants of the SGP30 MOX sensor, named SGP30.1, SGP30.2, SGP30.3, SGP30.4 with different configurations of hot plate temperatures and different membranes were provided by Sensirion as possible candidates for the series product.

Furthermore, a reference sensor box, equipped with a selection of sensors of Table 1 and Table 2 was manufactured by UnravelTEC. The sensor box consisted of (i) a SPEC Sensors

Klima- und Energiefonds des Bundes – Abwicklung durch die Österreichische Forschungsförderungsgesellschaft FFG

O3 sensor (DGS-O3), with a 1:1 cross-sensitivity to NO2, (ii) an Alphasense NO2 sensor (NO2-A43F), (iii) an Alphasense NO sensor, (iv) a Sensirion SCD 30 CO2 sensor and an environmental sensor (Bosch BME-280).

A test of the MOX sensor variants showed that some configurations show a high sensitivity (but not selectivity) to NO2 (cf. Table 3). Real-world tests also showed that some configurations are also sensitive to reducing gases such as NO, NH₃, H and CO. Since the tracer gas should be distinguishable from cross-interfering gases, possibly contained in the ambient air, the maximum sensor response (ticks) was recorded under laboratory conditions with NO2 and under real-world conditions. The maximum ticks for quick concentration changes are shown in Table 3.

Table 3: Sensors for sensor board 1 (series product).

MOX	SIGNAL CHANGE	SIGNAL CHANGE	MAX. SIGNAL CHANGE
SENSOR	LABORATORY 606	LABORATORY 19.2	ENVIRONMENT (TICKS)
CONFIG.	PPB NO2 (TICKS)	PPM NO2 (TICKS)	
SGP30.1	-	-	1020
SGP30.2	2130	8870	-
SGP30.3	4280	11250	1910
SGP30.4	37808	42628	1380

The tests with the reference sensor box showed that both the Alphasense NO2-A43F NO2 sensor and the Alphasense NO-A4 NO sensor showed good agreement with the reference instruments, accompanied by a small drift (60 seconds averaging period). The combined NO₂/O₃ sensor (SPEC Sensors DGS-O3) also showed good correlation with the reference. However, the sensor reading was only reliable for 30 min averaging period, which is too long for the series product.

An interesting tracer gas is Thiols currently investigated by PCCL. The absorption spectrum of Thiols appears to allow the adoption of a previously developed miniature fiber-coupled optothermal sensor as a reference sensor to measure Thiols. This will be investigated further.

3.2 Development of a functional polymer

During the last reporting year, a detailed study of the thermal properties of Generation 1 samples (PU+ABCN and PU+AIBN) was carried out. Further focus was put on studying the effect of the ageing on their thermal response. Generation 1 was finally subjected to mechanical and electrical tests.

Klima- und Energiefonds des Bundes – Abwicklung durch die Österreichische Forschungsförderungsgesellschaft FFG

Lastly, a new formulation based on Generation 2 was developed using dendritic polyols and examined by TGA and DSC tests to analyse the gas release temperatures. This approach allowed a higher binding of thiols molecules to the polymer matrix, resulting in a higher release of tracer gases at critical temperatures.

3.2.1 Generation 1

3.2.1.1 Sample preparation

ABCN and AIBN were incorporated into a polymeric matrix formulated with Lupranol 2095 and Desmodur 44 V70L in a stoichiometric ratio of hydroxyl to isocyanate groups. DBN (0,1 wt. %) was used as catalyst. The individual components and the corresponding blowing agents (4.5 wt. %) were added to 20 ml vial and homogenized in a vortex mixer VM-200 (StateMix Ltd., Canada), producing two formulations, PU-ABCN and PU-AIBN. The curing of the samples was done in aluminium pans in a standard convection oven at 40 °C. A polyurethane coating (PU) without any blowing agent was also produce as reference.

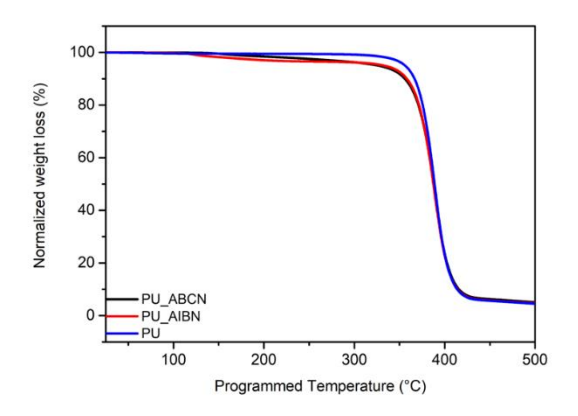
The full curing of the samples was confirmed by FTIR measurements (16 scans with a resolution of 4 cm⁻¹) due total disappearance of the characteristic and strong isocyanate band at 2270 cm⁻¹ after applying the curing conditions.

3.2.1.2 Thermal characterisation

Thermogravimetric analysis (TGA)

TGA tests were done from 25°C to 900°C with a constant heating rate of 10°C/min under inert (N₂) atmosphere. TGA tests showed a first decomposition step for PU-ABCN starting at 136 °C (onset temperature) and at 119 °C (onset temperature) for PU-AIBN. This first decomposition was not observed in the pure polyurethane coating, which proves the proper incorporation of the blowing agents into the polyurethane matrix. Moreover, the first derivative of the TGA curves (differential thermogravimetry, DTG) of PU-ABCN showed peak temperatures for the highest rate of thermal degradation at 147 °C and 252 °C, while the DTG of PU-AIBN exhibited peak temperatures of 116 °C and 185 °C (Figure 1).

Klima- und Energiefonds des Bundes – Abwicklung durch die Österreichische Forschungsförderungsgesellschaft FFG



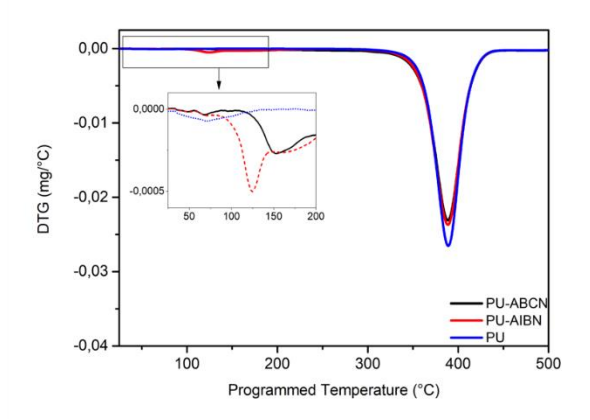


Figure 1: TGA and DTG curves of the developed polymer formulations.

Thermal desorption - Gas chromatography/mass spectrometry (TD-GC/MS)

For TD-GC/MS tests, samples were heated up from 60 °C to 200°C with a constant rate of 10 K/min. The decomposition products were ionized with an energy of 70 eV and scanned within the range of 10-200 m/z. The peak temperatures (161 °C for PU-ABCN and 120 °C for PU-AIBN) determined from the TD-GC curves indicate the temperatures at which the maximum release of volatile compounds happens. As expected, due to the high decomposition temperature of the matrix, the pure polyurethane sample does not show any peak temperature in the studied temperature range (Figure 2).

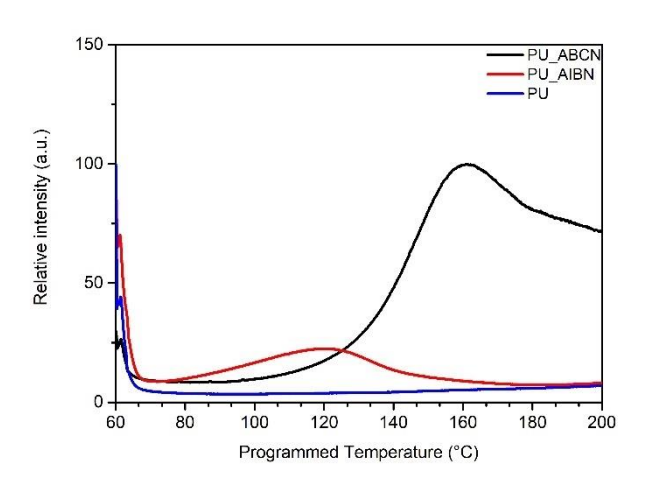


Figure 2: TD-GC chromatograms of the formulations.

On the other hand, in the mass to charge ratio graphs of PU-ABCN, a signal at (m/z) 109 was observed emerging at a desorption temperature of approximately 110 °C to 120 °C. This characteristic signal is assigned to cyclohexane carbonitrile, the main product during the thermally induced decomposition of ABCN. At higher temperatures other characteristic signals such as cyclohexene (m/z 82), methacrylonitrile (m/z 67) and 1-propene (m/z 41) can be observed due to further fragmentations. In contrast, PU-AIBN showed already at 70-80°C a characteristic signal at an m/z ratio of 69. This correlates with isobutyronitrile species, which

Klima- und Energiefonds des Bundes – Abwicklung durch die Österreichische Forschungsförderungsgesellschaft FFG

at higher temperatures produces ethenimine (m/z 54) and 1-propane (m/z 41) species (Figure 3).

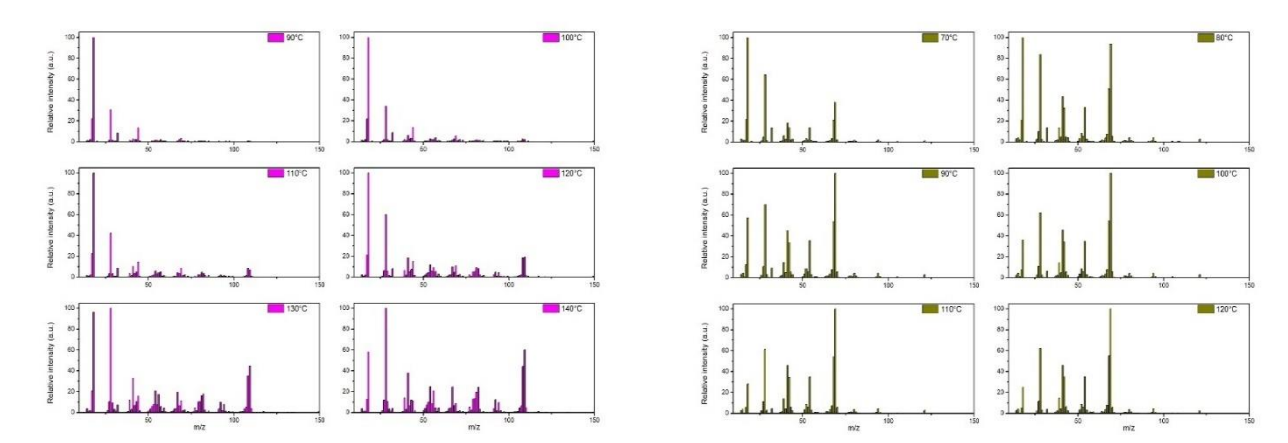


Figure 3: Mass spectra of volatile decomposition products of PU-ABCN and PU-AIBN.

<u>Differential scanning calorimetry (DSC)</u>

DSC measurements were performed from 15° C to 200° C with a heating rate of 10° C/min under N_2 atmosphere. The decomposition of the blowing agents present in the matrix can be observed as an exothermic reaction due to the release of the volatile species. PU-ABCN showed a decomposition peak temperature of 155° C, while PU-AIBN presented a peak of 131° C. These values are in good correlation with the previously measured values. As also expected, the pure polyurethane sample did not show any exothermal signal during the studied temperature (Figure 4).

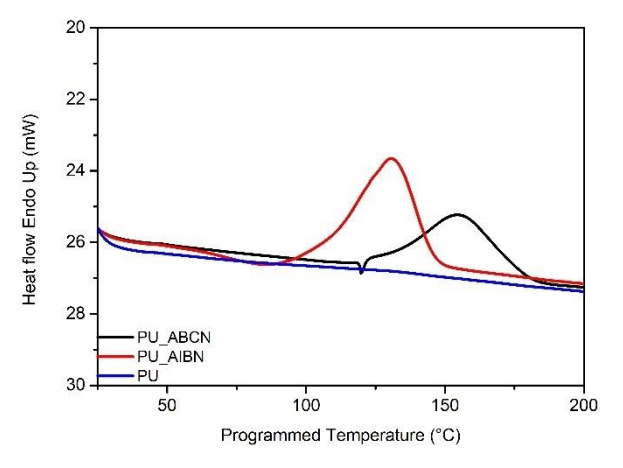


Figure 4: DSC curves of the formulations.

Klima- und Energiefonds des Bundes – Abwicklung durch die Österreichische Forschungsförderungsgesellschaft FFG

3.2.1.3 Ageing tests

Different PU-ABCN, PU-AIBN and PU samples were aged over six months at room temperature, 40 °C, 50°C and 60°C using standards convection ovens. The weight of the samples was periodically monitored every seven days in order to study the decomposition of the blowing agents. Two samples of each formulation were used as weight control for every condition to have a statistical result. The effect of the ageing on the decomposition after 3, 7, 21, 42, 84 and 183 days was also investigated by DSC. For DSC tests, six samples of each formulation were aged at every temperature and tested after the mentioned days.

PU-ABCN

PU-ABCN samples aged at RT did not show a significantly weight loss during the ageing studies (Figure 5). This was confirmed by DSC studies, in which the peak temperatures were always either 155 °C or 156 °C and the exothermal enthalpy showed similar values at every testing time (Figure 6). However, at 40°C, PU-ABCN samples showed a moderate weight loss over time. Considering that the content of ABCN in the sample was 4.5 wt.%, there was still around 33 % of the initial ABCN left after six months at 40 °C. This decrease of weight could be also observed in DSC experiments, where the decomposition enthalpy value decreased over time as the weight of the blowing agent in the formulation does. The temperature peak values (155 °C) remained the same at every testing time (Figure 6). Similar behaviour could be observed for PU-ABCN aged at 50 °C, in which there was still around 33% of ABCN left after six months. A decrease of the decomposition of enthalpy could also be noticed over time. Nevertheless, the temperature peak values did not change, showing similar values (155 °C) (Figure 6). PU-ABCN samples aged at 60 °C showed a faster decomposition rate than PU-ABCN samples aged at RT, 40°C and 50°C. ABCN included in the matrix was fully decomposed after 100 days, as it can be seen in Figure 6, when the weight loss reaches the plateau of 95.5 %. DSC tests proved the full decomposition after six months since no decomposition enthalpy could be observed. The high decomposition of ABCN after 84 days was also noticeable by DSC tests, where the decomposition enthalpy was very low and where the peak temperature value was shifted to the right as consequence of the small amount left of ABCN (Figure 6).

Klima- und Energiefonds des Bundes – Abwicklung durch die Österreichische Forschungsförderungsgesellschaft FFG

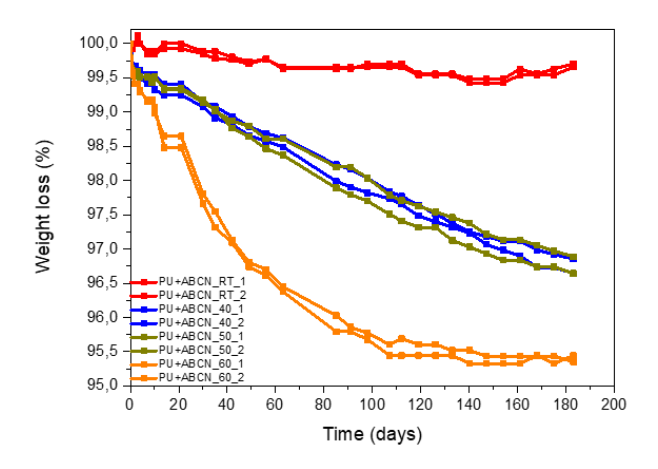


Figure 5: Weight loss vs. time of PU-ABCN aged samples.

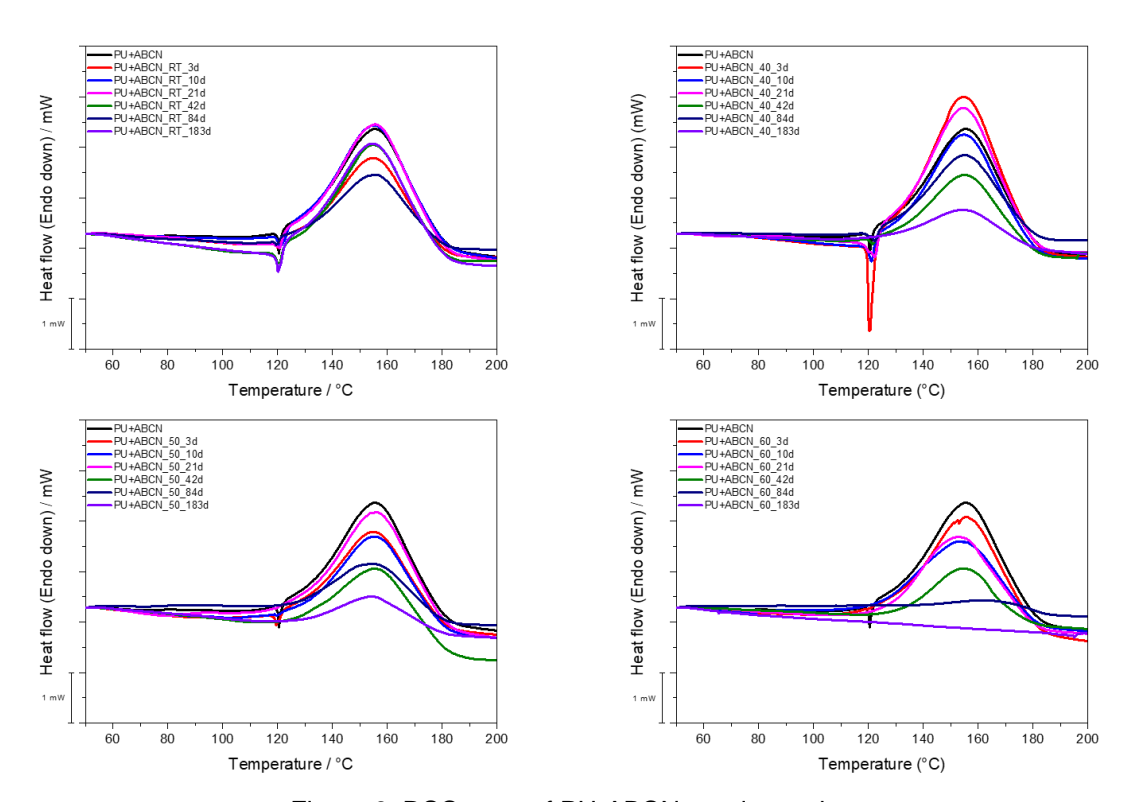


Figure 6: DSC tests of PU-ABCN aged samples.

PU-AIBN

PU-AIBN samples aged at RT showed similar behaviour as PU-ABCN at 60 °C. Even though the content of AIBN in the samples was theoretically 4.5 wt.%, the plateau (meaning a full decomposition of AIBN) was reached here at 96.5 % and 96 % (Figure 7). This could be due to an early decomposition of AIBN during the curing process of the samples and/or to a non-homogeneously distribution of the AIBN in the matrix. DSC curves confirmed the full decomposition of the AIBN after 84 days as can be observed in the graphics where there was not decomposition enthalpy for the tests performed after 84 and 183 days (Figure 8). On the

Klima- und Energiefonds des Bundes – Abwicklung durch die Österreichische Forschungsförderungsgesellschaft FFG

other hand, PU-AIBN samples aged at 40 °C presented a much faster decomposition of AIBN, reaching a total decomposition after 10 days as can be seen in the weight loss graphic. The full decomposition plateau was reached between 96 % and 97 %. As in the previous case, it could be explained due to a non-proper distribution of AIBN in the polyurethane matrix or to a decomposition during the curing of the matrix. DSC tests were just significant for the sample aged during three days, where a remaining enthalpy of decomposition was observed. A small shift to the right of the temperature peak could be noticed after three days (Figure 8). PU-AIBN samples aged at 50 °C behaved in a similar way, showing a full AIBN decomposition after 10 days. It could be clearly noted in both graphs, especially on DSC curves, where also a significant decrease of the decomposition enthalpy and a right shift of the peak temperature were already observed after three days (Figure 8). Finally, PU-AIBN samples aged at 60 °C showed the fastest decomposition rate. In this study-case, the plateau has been already reached around ten days. Just a very small enthalpy of decomposition curve and a considerable peak temperature (162 °C and 164 °C, respectively) could be noted after three and ten days in DSC tests (Figure 8).

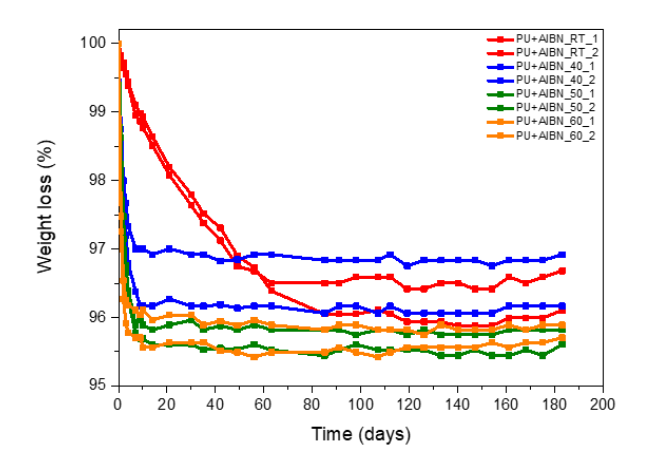


Figure 7: Weight loss vs. time of PU-AIBN aged samples.

Klima- und Energiefonds des Bundes – Abwicklung durch die Österreichische Forschungsförderungsgesellschaft FFG

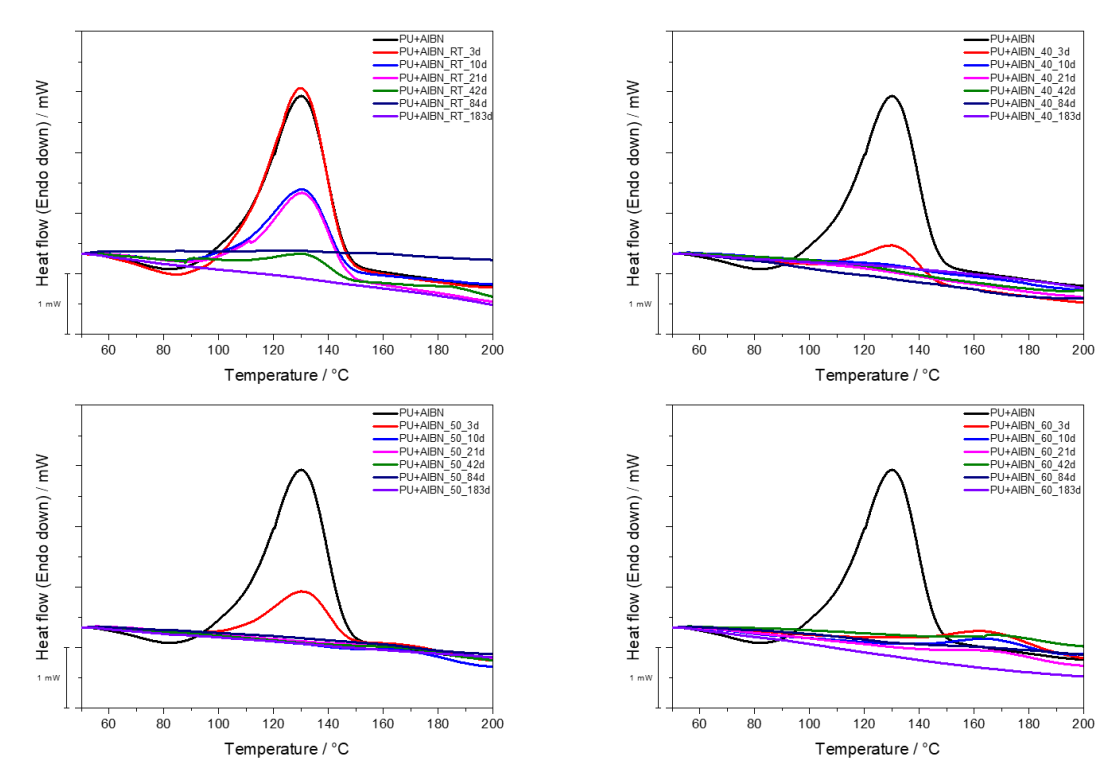


Figure 8: DSC tests of PU-AIBN aged samples.

Unlike PU-AIBN aged samples, at same conditioning times PU-ABCN aged samples present a linear tendency to lose weight as the temperature increases in a mild range, as can be seen in Figure 9.

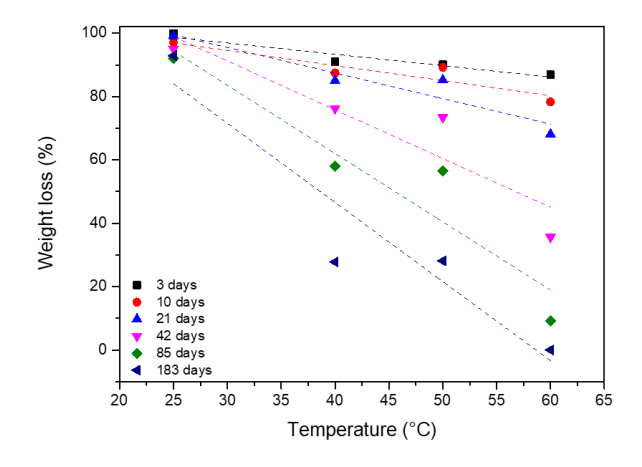


Figure 9: Weight loss vs. temperature of PU-ABCN aged samples at different times.

Pure PU

Pure PU samples did not show any relevant weight loss during the six months (Figure 10).

Klima- und Energiefonds des Bundes – Abwicklung durch die Österreichische Forschungsförderungsgesellschaft FFG

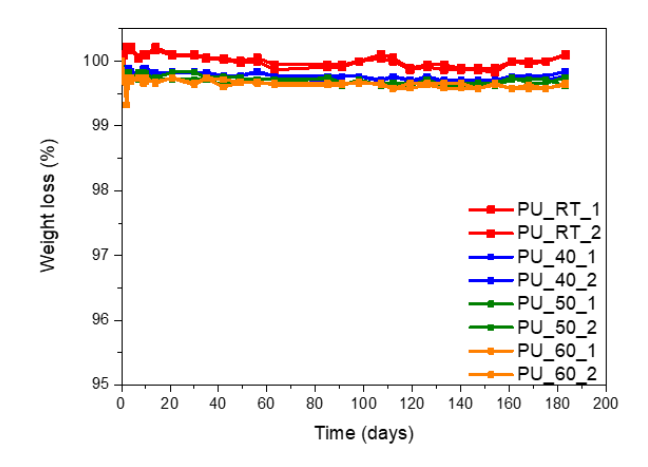


Figure 10: Weight loss vs. time of pure PU aged samples.

3.2.1.4 Mechanical tests

Mechanical tests to measure the hardness and Young's modulus of pure PU, PU+ABCN and PU+AIBN samples were conducted using an Anton Paar UNHT3 Nanoindenter. Unfortunately, as consequence of the uneven surface, the stickiness of the samples and the very low estimated modulus, non-proper mechanical values could be measured.

3.2.1.5 Electrical tests

The electrical conductivity of Generation 1 samples was studied using a Fluke 3000 FC Series Wirles Multimeter. No values were observed when measuring pure PU, PU+ABCN and PU+AIBN samples, meaning that the addition of ABCN and AIBN to the matrix did not have an impact on the electrical conductivity of the polymeric coating. Therefore, the three formulations could be considered as electrical isolators.

3.2.2 Generation 2

3.2.2.1 Sample preparation

New formulations based on Generation 2 samples were synthesized using a six-functional dendritic polyol (Boltorn[™] H2004) provided by Perstorp, a polymeric MDI (pMDI) provided by Covestro (Desmodur® VL R 20), 1-propanethiol provided by Merck and DBN (provided by Merck) as catalyst. Three different formulations were synthesized following different stoichiometric ratios and cured at 40°C.

CC_01: prepared without 1-propanethiol and used as a reference.

DD_01: 50% of the NCO groups of the polymeric MDI were reacted with 1-propanethiol.

EE_01: More of the 50% of the NCO groups of the polymeric MDI were reacted with 1-propanethiol.

Klima- und Energiefonds des Bundes – Abwicklung durch die Österreichische Forschungsförderungsgesellschaft FFG

As showed in Figure 11, the full reaction and the coupling of 1-propanethiol to the PU matrix could be proved by the disappearance of the characteristic NCO band in the range of at 2270 cm⁻¹ and the presence of a band at 1685 cm⁻¹ respectively.

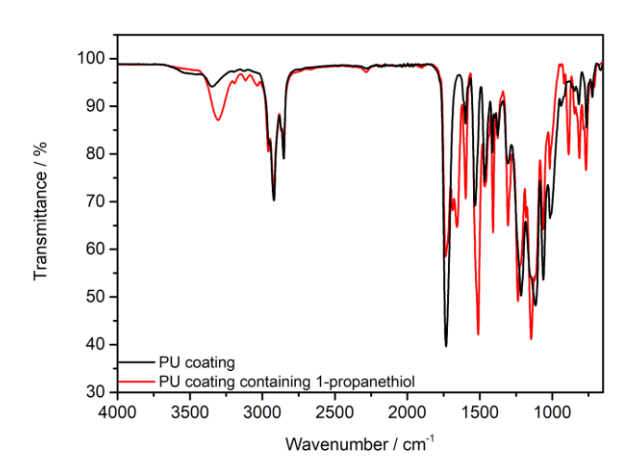


Figure 11: FTIR spectrum of cured CC 01 and DD 01.

3.2.2.2 Thermal characterisation

Thermogravimetric analysis (TGA)

TGA tests were done from 25° C to 900° C with a constant heating rate of 10° C/min under inert (N₂) atmosphere. An earlier onset temperature (140° C) was observed for samples containing 1-propanethiol, where moreover, three decomposition steps could be seen. It was also noticed that the higher the amount of 1-propanethiol, the lower the decomposition temperature (Figure 12).

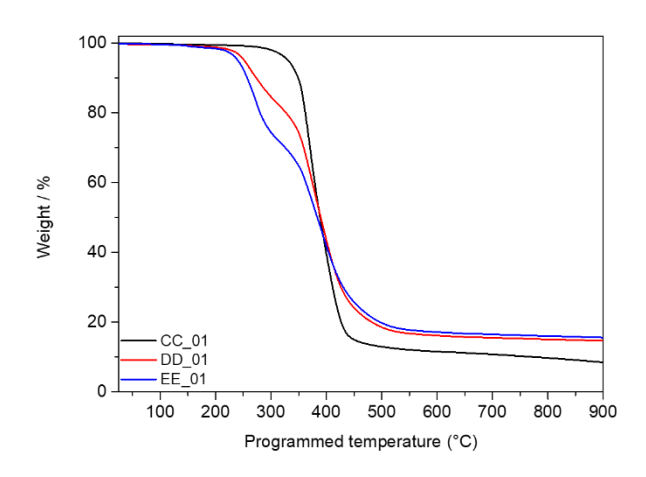


Figure 12: TGA curves of CC_01, DD_01 and EE_01.

Differential scanning calorimetry (DSC)

DSC measurements were performed from 25°C to 200°C with a heating rate of 10°C/min under N₂ atmosphere. The endothermal response, correlated to the release of 1-propanethiol, was

Klima- und Energiefonds des Bundes — Abwicklung durch die Österreichische Forschungsförderungsgesellschaft FFG

clearly observed for samples DD_01 and EE_01 with temperature peak values of 164°C and 160°C respectively. The effect of a higher amount of 1-propanethiol could be noticed with a more intense endothermal signal (Figure 13).

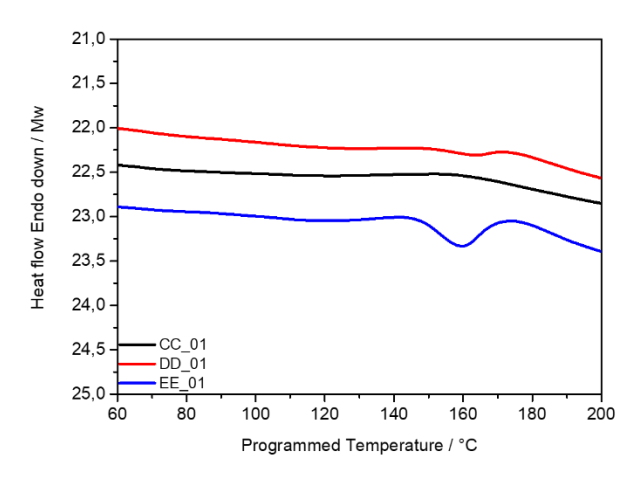


Figure 13: DSC curves of CC_01, DD_01 and EE_01.

3.3 Adaption of sensor technologies

3.3.1 System design

The proposed system design that was developed during the project work of GALION consists of the following three components:

- 1. A MOx based gas sensor with four differently configured sensor pixels
- 2. An operation configuration of the four pixels
- 3. A data processing scheme with a warning signal as output

The pure hardware component which fulfils the application requirements is the Sensirion gas sensor platform, SGP4x, as presented in Figure 14. The used senor is an engineering version of the commercially available product SGP40 allowing for free access to all configuration and read-out settings which are otherwise fixed.

To overcome the generally low selectivity of individual MOx sensors we decided to use a fourpixel MOx sensor platform which combines four separately controllable MOx-sensors in a single package. In this way it was possible to configure some of the sensor pixels in such a way that the released target molecules show fingerprints for the investigated materials that are distinguishable from the fingerprints of various background compounds or competing gases that could occur in real use-case applications. A summary of the implemented material combinations and operation properties of the used MOx-sensor pixels is provided in Table 4.

Klima- und Energiefonds des Bundes — Abwicklung durch die Österreichische Forschungsförderungsgesellschaft FFG

Finally, the data processing step is necessary to evaluate the recorded raw data such as to achieve an early warning signal indicating the upcoming of a critical battery state. A detailed description of this algorithm follows below.

	Base	Dopant	Operation	Operation
	Material		Temperature	Mode
Pixel 1	-	-	-	-
(not used)				
Pixel 2	In ₂ O ₃	none	350°C	continuous
Pixel 3	SnO ₂	Pd	350°C	continuous
Pixel 4	WO ₃	Pt	250°C	continuous

Table 4 - Sensor pixel properties of the SGP4x platform used in this study.

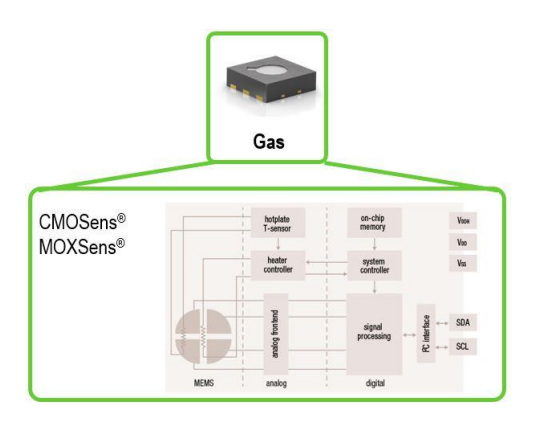


Figure 14: Picture and schematics of the four pixel gas sensor with digital I2C interface used in the GALION project.

3.3.2 Multi-pixel gas sensor for selective detection of critical battery states

The selective detection of cleavage products in real-time is a key function to trigger a warning against an overheating event as early as possible. However, in view of potential applications such as in electric vehicles, particular attention must be paid on identifying possible false positive alert triggers. Here we explore the following events as potential false triggers that are not related to high-temperature events. Concerning outdoor applications, it is possible that exhaust gases from combustion engines reach the gas sensor. Among those, nitrogen oxides (NOx), hydrogen (H₂), and carbon monoxide (CO) are typical candidates of significant abundance in the low ppm range. In the case of indoor applications, the list is completed by a series of volatile organic compounds (VOCs), for instance originating from outgassing materials or bio-effluents. Note that CO2 which is a gaseous compound of relatively high concentration is not considered here because the MOx sensor pixels used in this study are insensitive to it. However, changes of water vapor concentrations, herein referred to as relative humidity (% RH), must be considered as a potential trigger event. In this study we defined

Klima- und Energiefonds des Bundes – Abwicklung durch die Österreichische Forschungsförderungsgesellschaft FFG

realistic concentrations of those competing gases to scale between 0.2 to 1.6 ppm for NO₂ (proxy for both, NO and NO₂), 2.0 to 16 ppm for H₂ or CO, and 1.0 to 8 ppm for ethanol (EtOH, proxy for VOCs). The relative humidity varied between 10% and 90%.

Using the gas mixing setup presented in Figure 15, we sequentially simulate first an overheating event with one of the functional polymers and thereafter the presence of the potentially interfering gas compounds. The responses of the three MOx sensor pixels during this sequence is depicted in Figure 16 (top row) for the coating system with 4.5 wt.% ABCN in a PU matrix. During the first period the functional coating material inside the heating chamber is heated up at 10 K/min until approximately 235°C and thereafter left unheated to cool down to room temperature (see black dashed line in Figure 16, top row). The gas measurement system constantly flushes clean air through the heating chamber and thereby transports the outgassing compounds to the sensor chamber causing strong yet quantitatively different sensor responses of all three pixels (light green span in Figure 16). After this period the gas measurement continuous with providing selected concentration steps of competing gas compounds including NO₂, H₂, CO and EtOH plus mixtures thereof (further colored areas in Figure 16). Note, that sensor responses are provided in ticks which represent the output of a 16-bit analog-digital converter (ADC) of a logarithmically scaled amplifier. As such the sensor responses used herein can be considered proportional to the materials resistivity which in turn scales approximately linearly with the logarithm of gas concentrations.



Figure 15 - Schematic illustration of the experimental setup. The gas mixing system serves as supply for a carrier air stream and accurate gas concentrations or mixtures thereof. Inside the heating chamber a functional polymer sample can be heated with feedback-controlled temperature gradient of 10K/min. The sensor chamber allows for a parallel read-out of up to 32 digital gas sensors.

Klima- und Energiefonds des Bundes – Abwicklung durch die Österreichische Forschungsförderungsgesellschaft FFG

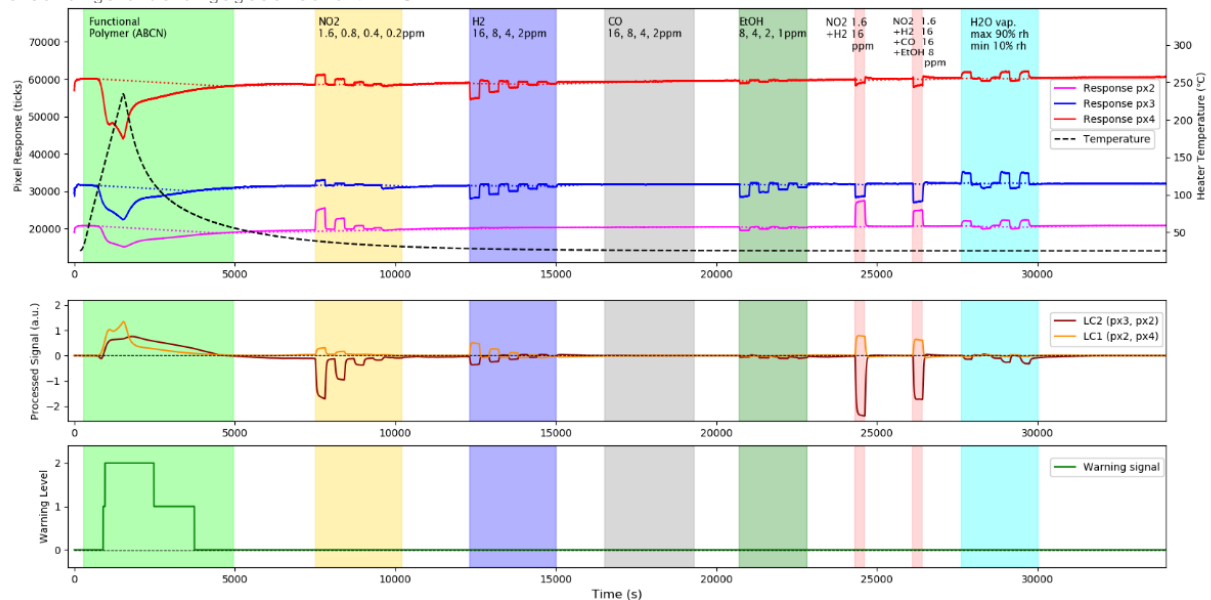


Figure 16 - Warning algorithm for the functional coating including ABCN in a PU-matrix. Top row: Raw responses of the 3 pixels of the SGP4x gas sensor in the presence of the target molecules released from the functional polymer upon heating (light green span) plus other competitor gases (spans with various colors). Middle row: Processed linear combinations of the raw sensor pixel traces using pixel 2 and 4 (LC 1, orange) and pixel 3 and 2 (LC 2, dark red) as input, respectively. Bottom row: Processed warning signal which selectively indicates the presence of the target molecules.

3.3.3 Warning signal algorithm

In the following we introduce an algorithmic scheme that allows us to selectively and reliably recognize the presence of the target molecules which are released when PU coating samples including AIBN or ABCN as functional additives are heated up. The first step of the warning signal algorithm consists of computing the baseline of each individual sensor pixel because only relative changes of the MOx sensor pixels are considered as meaningful information. Herein, we apply the following simple yet efficient method: The sensor pixel value at each point in time S_i is compared to the latest computed baseline value BL_{i-1} to obtain the current difference between sensor value and baseline value. If this difference is within predefined limits the new baseline value is equal to the current sensor value. Otherwise, if the difference exceeds the maximum or minimum allowed limit, the new baseline value is calculated such that it follows the sensor trace with a maximum or minimum gradient (Equation 1).

Equation 1

$$BL_i = \left\{ \begin{array}{ccc} S_i & , & S_i - BL_{i-1} < pos \ limit \ and > neg \ limit \\ BL_{i-1} + MPG & , & S_i - BL_{i-1} > pos \ limit \\ BL_{i-1} + MNG & , & S_i - BL_{i-1} < neg \ limit \end{array} \right.$$

Where BL_{i-1} and BL_i are, respectively, the previous and the current baseline values, S_i is the current sensor pixel value and MPG (maximum positive gradient), MNG (maximum negative

Klima- und Energiefonds des Bundes – Abwicklung durch die Österreichische Forschungsförderungsgesellschaft FFG

gradient) are the predefined limits to restrict the baseline gradient in upwards and downwards direction. The resulting baseline traces for sensor pixels 2, 3, and 4 are added as colored dashed lines in Figure 16 (top row) directly underneath the sensor pixel traces. The sensor traces relative to their baseline trace undergo downwards amplitudes in the presence of reducing gases (e.g. H₂, CO, EtOH) and upwards amplitudes in the presence of oxidizing gases (e.g. NO₂). Note that the sensor responses to CO are extremely weak and therefore hardly visible in our system. Obviously, the sensor responses of all pixels to the target molecules exclusively show clear downwards amplitudes. Thus, in the second step of the algorithm, all sensor pixel responses with upwards amplitudes are discarded from a warning signal by assigning zeros to the warning signal trace when any of the 3 sensor pixels outputs a positive value with respect to its baseline (Equation 2).

Equation 2

$$WS1_i = \left\{ \begin{array}{ccc} 0 \ , & S_{Px2,i} - BL_{Px2,i} > 0 \ or \\ & S_{Px3,i} - BL_{Px3,i} > 0 \ or \\ & S_{Px4,i} - BL_{Px4,i} > 0 \\ 1 \ , & elsewhere \end{array} \right.$$

Where WS1_i (sub-warning signal 1) denotes one subcomponent of the warning signal, S_{PxN,i} and BL_{PxN,i} refer to the sensor pixel response and the baseline value of each pixel.

In the third step we compute two specific linear combinations of the sensor traces to extract additional information from the relative quantities of the sensor amplitudes at a given gas composition. Linear combination 1 is obtained using sensor pixels 2 and 4 (Equation 3) and linear combination 2 is computed based on sensor pixels 2 and 3 (Equation 4).

Equation 3

$$LC1 = S_{Px2,i} - 1.2 \times S_{Px4,i}$$

Equation 4

$$LC2 = S_{Px3,i} - 3 \times S_{Px2,i}$$

The new sensor trace LC1 shows upwards amplitudes during the heating period of the functional polymer as well as during the supply of NO₂ and H₂. However, during the supply of CO, EtOH, and water the computed trace shows downwards amplitudes (dark red trace in Figure 16, middle row). Thus, we reach a partial selectivity between the two groups of gases or gas compositions. The second linear combination shows upwards amplitudes during the heating of the functional polymer as well as during the supply of EtOH and water while we create downwards amplitudes in the case of NO₂, and H₂ (orange trace in Figure 16, middle

Klima- und Energiefonds des Bundes – Abwicklung durch die Österreichische Forschungsförderungsgesellschaft FFG

row). Thanks to those two linear combinations we achieve a discrimination of the target molecules being released during the heating of the functional polymer from the competing gases. Whenever linear combination 1 multiplied with linear combination 2 displays negative values we can be sure that the sensor reacts to something other than the target molecules. Thus, a warning signal indicating the presence of the target molecules requires that linear combination 1 multiplied with linear combination 2 be positive. Finally, we suggest defining two warning levels apart from zero, level 1 and level 2 which are reached when the product of the 2 linear combinations exceeds threshold 1 and threshold 2, respectively:

Equation 5

$$WS2_i = \left\{ \begin{array}{ccc} 0 & , & LC1 \times LC2 & \leq threshold1 \\ 1 & , & threshold1 < LC1 \times LC2 < threshold2 \\ 2 & , & LC1 \times LC2 > threshold2 \end{array} \right.$$

Where WS2_i (sub-warning signal 2) denotes the second subcomponent of the warning signal As such warning level 1 can be configured as a very sensitive and fast measure indicating the thread of an overheating event. Level 2, however, could be set to represent a less sensitive but very robust and unambiguous indication or confirmation of such an overheating event. This means, in addition to the qualitative discrimination, we also exploit the fact that the target molecules reach significantly higher quantities as typical competing gases or other potentially interfering compounds. We are aware that false positives could arise at warning level 1 due to its low threshold and the resulting high sensitivity to gas compositions that by coincidence can have similar sensor response characteristics like the target molecules. However, in warning level 2 the threshold is chosen such that only sufficiently strong sensor responses are detected which reduces the probability of false positives to a minimum. The final warning signal as it is displayed in Figure 16, bottom row, simply combines the subcomponents of the warning signal represented by Equation 2 and Equation 5 (with the latter one being the dominant part):

Equation 6

$$WS_i = WS1_i \times WS2_i$$

3.3.4 Onset temperature of the warning signal

The onset temperature at which the system allows a first warning of an overheating event is certainly the most crucial system parameter from an application point of view. An onset temperature in the range of 20°C to 40°C above the maximum operation temperature of the thermo-sensitive device would be desirable in most cases. In Figure 17 the warning signal's

Klima- und Energiefonds des Bundes – Abwicklung durch die Österreichische Forschungsförderungsgesellschaft FFG

robustness and reliability of the functional polymer systems is explored with respect to deviceto-device variations and material aging. A total of 25 gas sensor responses (each consisting of 3 pixels) were recorded and processed through the warning signal algorithm introduced above. The resulting traces are plotted as a function of the rising temperature inside the heating chamber to display the onset temperature distribution. As can be inferred from Figure 17 (top row) the onset temperatures of the system ABCN in PU-matrix are distributed from 115°C to 120°C whereas the system AIBN in PU-matrix (Figure 17 bottom row) shows onset temperatures in the range of 105°C to 110°C (fresh samples, dark green traces). If the PUmatrix with no functional additive is present, the algorithm detects the heating event only at around 160°C to 165°C (dark grey traces) due to the decomposition of the coating matrix. The observed temperature difference for a warning signal can be considered as the benefit of employing functionalized polymers (e.g. as coating of an electronic device) for the early detection of a critical overheating event. Depending on its application, this method could shorten the detection time of such critical events in the range of some minutes. A prominent example would be to implement this system inside Li-lon battery packs for electric vehicles to comply with upcoming safety standards in which a passenger warning is expected up to 5 minutes prior to dangerous situations inside the cabin. While robustness with respect to deviceto-device variation is very promising considering the narrow distribution of onset temperatures, we do observe a shift of the detection temperature caused by aging of coating samples. This behavior is expected, since azo-based blowing agents can show a decomposition already at moderate temperatures, although at a slower rate. The light cyan traces in Figure 17 reveal that storage at room temperature in an open environment (AIBN: 8 days, ABCN: 13 days) leads to a delay in the detection of the overheating event which is explained by quantitative effects. This means, slow decomposition of the additives during storage results in a reduction of the concentration of the blowing agent within the matrix so that higher temperatures are needed to release the necessary amount of target molecules.

Comparing the two functional polymer systems studied here it can be stated that while AIBN allows lower onset detection temperatures in freshly prepared samples, it is more susceptible to aging and decomposition at moderate temperatures than ABCN. Aged samples containing AIBN display an approximately 20°C higher onset temperature, aged ABCN samples a roughly 10°C higher onset temperature as compared to their initial fresh states. A further evaluation of the impact of aging effects and concepts to reduce the impact are subject of further research.

Klima- und Energiefonds des Bundes – Abwicklung durch die Österreichische Forschungsförderungsgesellschaft FFG

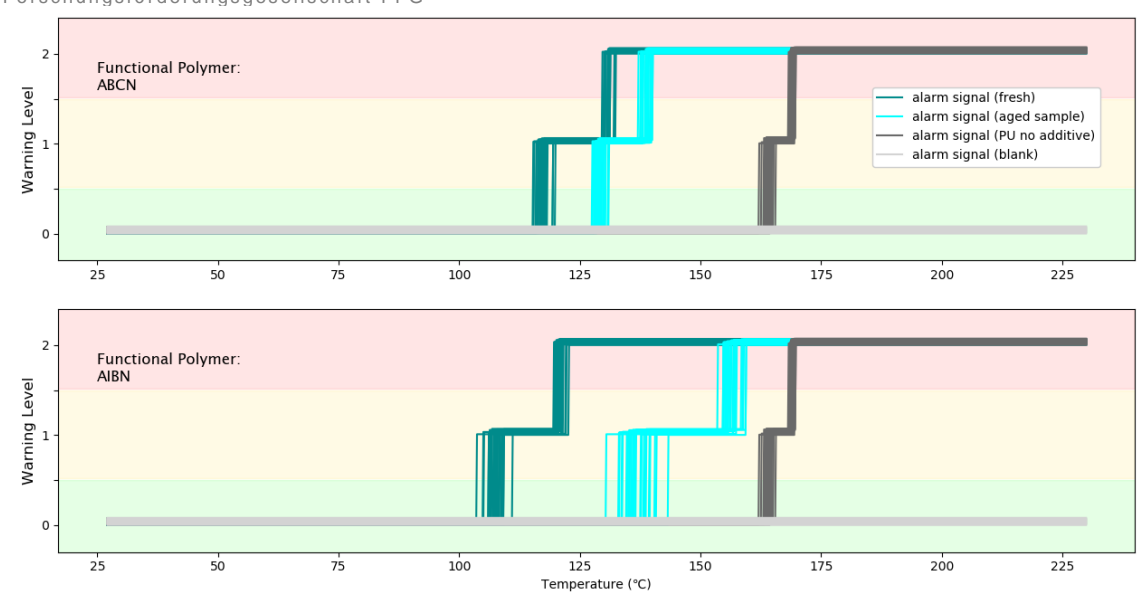


Figure 17 - Overlay of warning signal traces of 25 gas sensors for fresh (dark cyan) and aged (light cyan) functional polymer systems for ABCN (top row) and AIBN (bottom row). The dark grey traces result from heating the pure polyurethane (PU) matrix without blowing agents. No warning signal is triggered by heating up the empty heating chamber (light grey traces). Note that traces in this plot were incrementally shifted upwards to reach better visibility of the overlapping of the traces. Warning levels 0, 1, and 2 are visualized b the traffic light colors green, yellow, and red.

3.3.5 Prototype for a battery demonstrator

The above-described system of gas sensor, operation configuration, and warning algorithm is available at necessary numbers for further demonstrations. Once product development phases are reached, the operation configuration as well as the data processing scheme can be implemented directly within the on-chip processing unit (ASIC) of the gas sensor. However, at the current prototype phase the algorithm is implemented at the post-processing level on the read-out device. A *Python* implementation of the algorithm is available and can be used in a demonstrator setup as is. The I2C communication has been implemented by the consortium member 'UnravelTec' and is also ready to use.

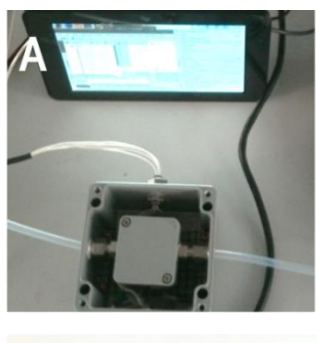
3.4 Validation of error detection

3.4.1 Heating setup

The experimental studies within the GALION project are mostly focussing on the concept of detection outgassing components upon a temperature rise in the range of room temperature up to over 200°C. The target temperature at which the final system shall work is around 80°C – 100°C, thus running experiments up to 150°C seems to be a reasonable starting point. Therefore, it was decided that Sensirion develops, builds, and provides three identical heating setups tailored for the requirements needed within the GALION project.

Klima- und Energiefonds des Bundes – Abwicklung durch die Österreichische Forschungsförderungsgesellschaft FFG

Figure 18: Next generation heating setups customized for the GALION project. A: Overview of heating system including chamber, tubing, power supply and control unit with screen. B: Downside view of the inner heating chamber with heater elements. C: Heating chamber with inner chamber for sample placement outer chamber for mechanical support and isolation material. Figure 18 shows photographs of the developed heating stage. It is a standalone system comprising heating stage, gas tubing connections, and a control unit allowing for feedback-loop controlled heating ramps ranging up to 20 K/min.



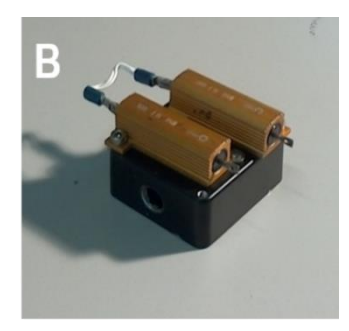




Figure 18: Next generation heating setups customized for the GALION project. A: Overview of heating system including chamber, tubing, power supply and control unit with screen. B: Downside view of the inner heating chamber with heater elements. C: Heating chamber with inner chamber for sample placement outer chamber for mechanical support and isolation material.

3.4.2 Setups to analyze electrolyte advection behavior

After a gas producing failure case inside the battery pack happens, the produced gas takes some time to reach the sensor. To investigate the gas distribution and time between gas production and trigger as well as to answer how the gas distribution is influenced by concentration, battery pack geometry and advection inside the pack, some improvisational setups were built and tested.

A principle test was conducted with a 1.87 m long tube with a diameter of 0.2 m (Figure 19). Two sensors were placed at the mid point and at the end of the tube. The end of the tube with the sensor was sealed off. On the other end a paper towel, which functions as the sample reservoir, was fixed to the inside of the tube. Subsequently the tube was sealed off with the possibility of sample injection using a syringe. The setup was used for general advection

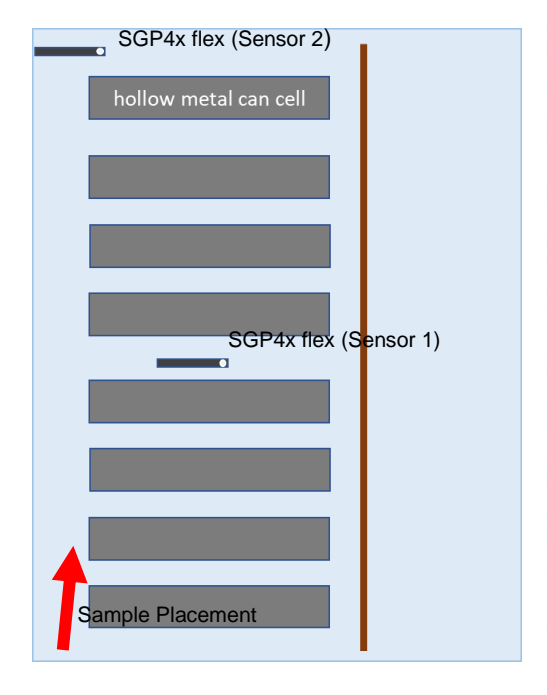
Klima- und Energiefonds des Bundes – Abwicklung durch die Österreichische Forschungsförderungsgesellschaft FFG

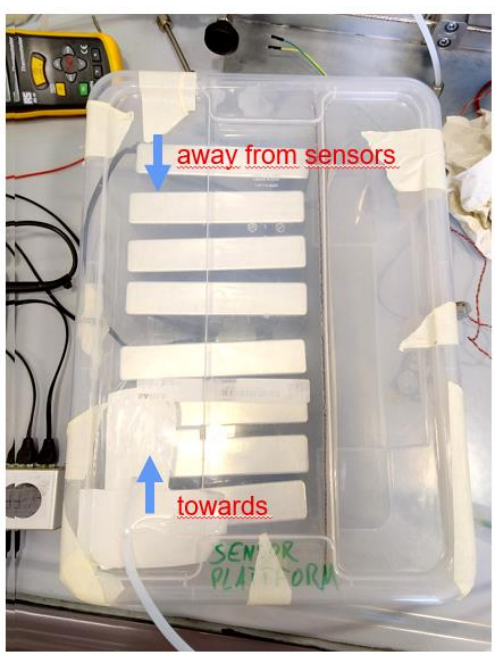
experiments of electrolyte without any ventilation or volume placeholders. The time between the injection and the last sensor signal was measured.



Figure 19: Experimental setup of the general advection experiments with line of sight from the injection point to the other end of the tube.

A simplified battery module was constructed out of an IKEA box and metal cans. The cans were arranged in the box as sketched in Figure 20 to replicate a simplified module. The volume was reduced to the side by a separator, made of carton. The sensors were labeled and arranged in the setup according to the sketch. The lid of the box was provided with two holes to fit the gas tube, which represents two different scenarios. The injection site remained at the same place for all the experiments, resulting in favorable and a non-favorable propagation direction due to the holes in the lid.



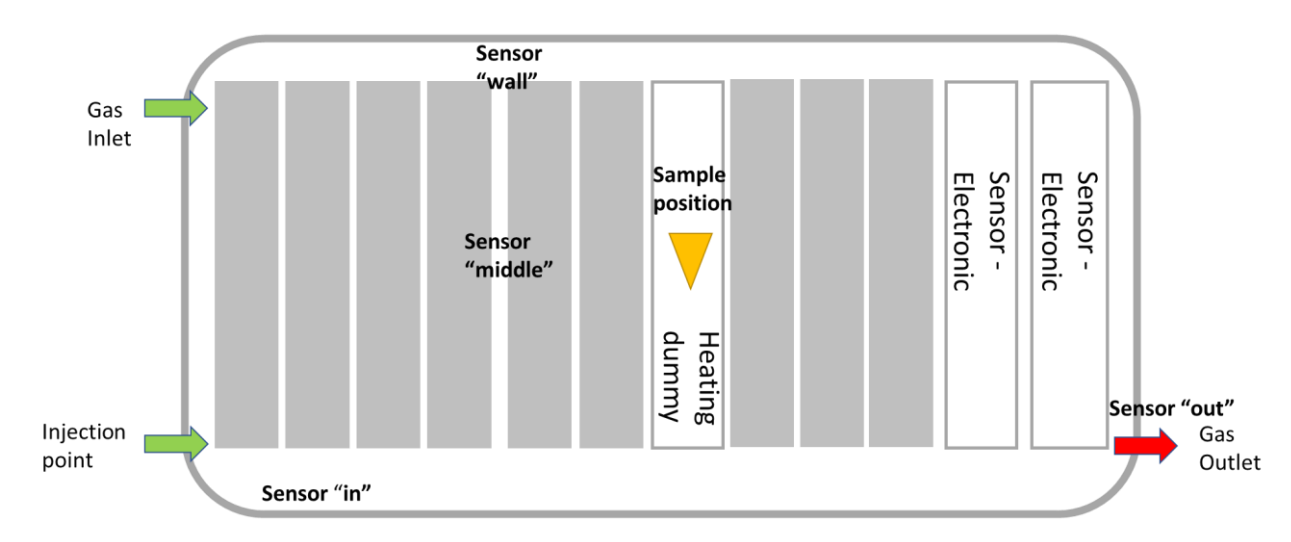


Klima- und Energiefonds des Bundes – Abwicklung durch die Österreichische Forschungsförderungsgesellschaft FFG

Figure 20: Setup of a simplified battery module for electrolyte advection experiments. Picture of the setup in the laboratory with two holes for the gas tube (right) and a sketch with the sensor placement within the setup (left).

A battery pack replica was constructed for demonstration purposes (Figure 21). The showcase is larger compared to commercially used battery packs, with a total volume of 10.3 l. The housing has 5 boreholes, one for the cables leading into the showcase and four as inlets/outlets. The lid of the showcase has two windows, which allow to see inside the pack replica. The interior is filled with 12 prismatic dummy cells, which represents the standard number of prismatic cells housed within a battery pack. Two of the dummy cells function as placeholders for the electronics needed to operate the sensors and the heating pad. One dummy cell is used as the heating dummy, which is equipped with a heating pad on the inside of the cell. In total of four sensors are placed within the showcase to detect the gas spreading.

Klima- und Energiefonds des Bundes – Abwicklung durch die Österreichische Forschungsförderungsgesellschaft FFG



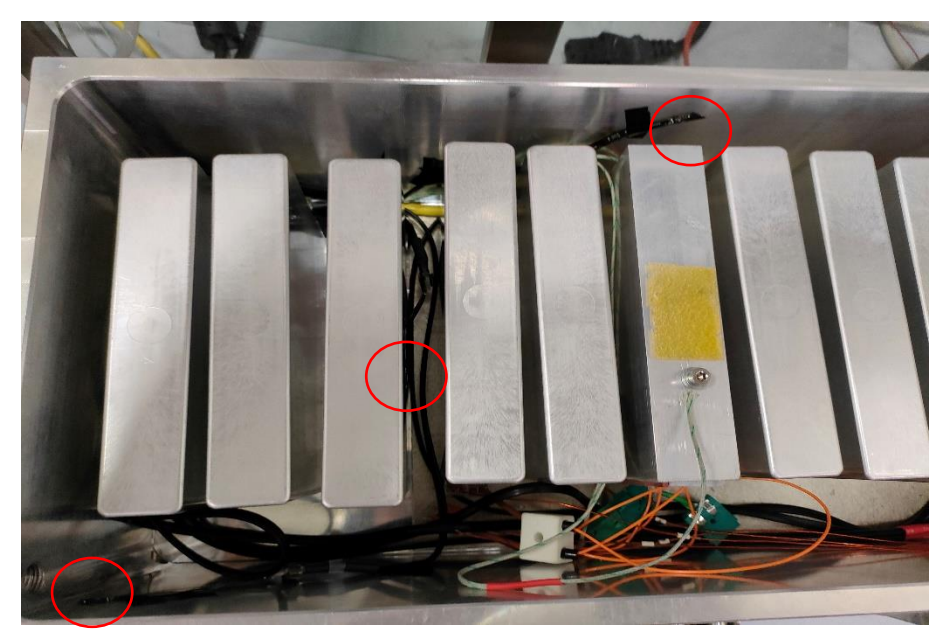


Figure 21: Setup of the showcase. Sketch with sensor positions, injection points and gas inlet and outlet (upper panel). Picture of the opened showcase with sample (yellow) placement and sensor positions (lower panel).

3.4.3 Degassing Temperatures of the polymer matrix

The generation 1 samples were investigated according to their degassing behavior related to the temperature and the amount of released tracer gas. To determine the decomposition of the polyurethane (PU) matrix, samples with no embedded additive were investigated as a reference experiment. The detection of the decomposition gases was registered by gas sensors.

A detailed analysis of selected sensors shows the decomposition temperature of the matrix (Figure 22). The selected sensors are the SGP30 and the SGP4x.

Klima- und Energiefonds des Bundes – Abwicklung durch die Österreichische Forschungsförderungsgesellschaft FFG

The decomposition temperature according to the SGP30 is slightly below 140 °C and according to the SGP4x it ranges from 135 to 140 °C. The temperature is well above the maximum target temperature of 120 °C suggesting thermal stability of the matrix.

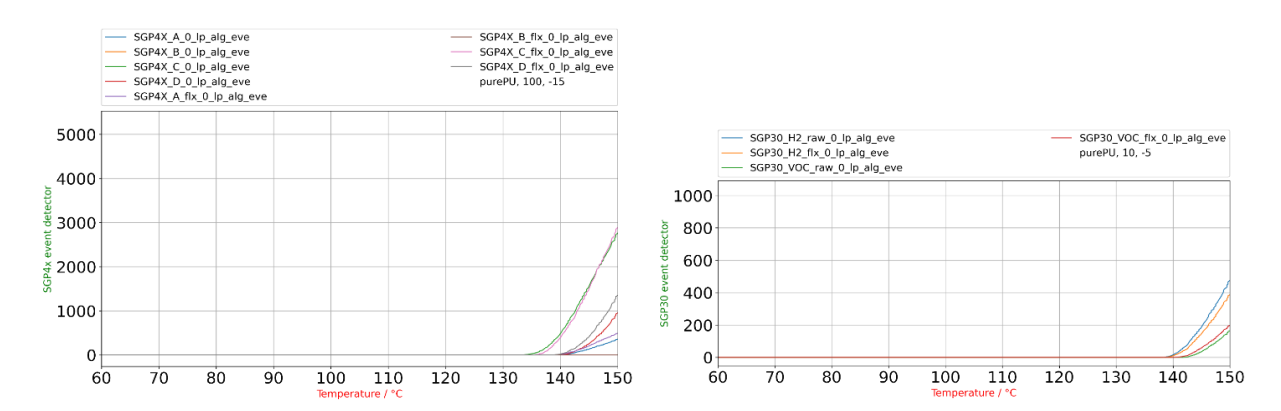


Figure 22: Detailed analysis of the decomposition temperature of the polymer matrix. Resulting temperature of the SGP4x (left) and the SGP30 (right).

3.4.4 Degassing Temperatures of the polymer tracer gases

The generation 1 polymers share the same matrix but were provided with two different additives. Gen 1.2 are embedded with ABCN or AIBN. Both additives show different release temperatures and an overall good detectability by the selected sensors.

Generation 1.2 samples with ABCN

A closer examination of the degassing temperature can be achieved by applying the event detector described in section 2.4. The selected sensors SGP30 and SGP4x have a good correlation regarding the degassing temperature (Figure 23). The different pixels on the SGP30 detect the tracer gas in a range of 118 °C to 123 °C. The SGP4x responds slightly earlier from 114 °C to 119 °C.

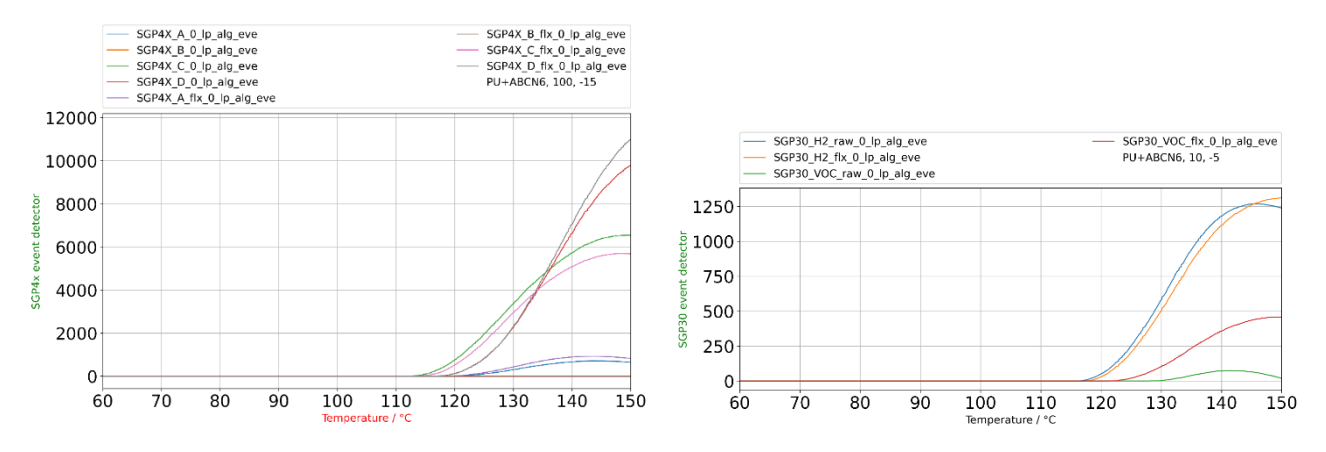
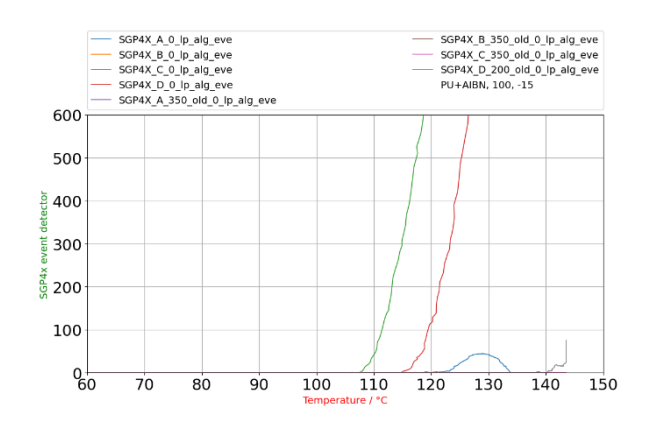


Figure 23: Detailed analysis of the decomposition temperature of the ABCN additive. Resulting temperature of the SGP4x (left) and the SGP30 (right).

Klima- und Energiefonds des Bundes — Abwicklung durch die Österreichische Forschungsförderungsgesellschaft FFG

Generation 1.2 samples with AIBN

The determination of the degassing temperature was achieved by applying the event detector described in section 2.4. The different pixels on the SGP30 detect the tracer gas in a range of 114 °C to 125 °C. The SGP4x responds slightly earlier from 108 °C to 120 °C (Figure 24). Overall, the selected sensors have a good correlation regarding the degassing temperature.



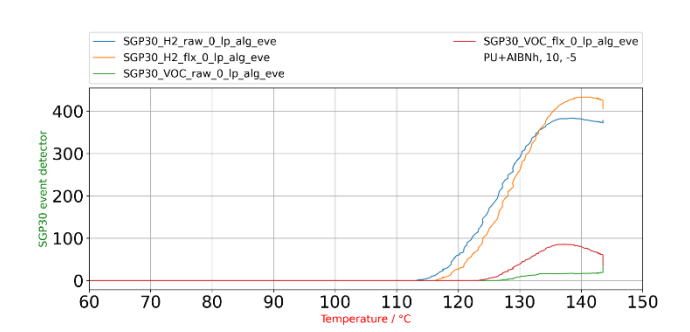


Figure 24: Detailed analysis of the decomposition temperature of the AIBN additive. Resulting temperature of the SGP4x (left) and the SGP30 (right).

3.4.5 Long-term stability of the polymers

An important factor for the application is the long-term stability of the polymer. Therefore, the stability of the bond between the matrix and the additive needs to be investigated. This property was examined by conducting aging tests. Such a test consists of a heat treatment at elevated temperatures over time. After different time periods, samples were removed from the oven and tested in the heating setup. The heating ramp for the testing of the long-term stability started at room temperature up to 150 °C at a rate of 10 K/min.

Aging effect of the ABCN additive

The aging affects the amount of additive bound to the PU matrix. The two main parameters to be determined are the detectability of the tracer gas and the release temperature. The samples of different aging states were compared to determine possible temperature shifts.

Despite the general shift to lower degassing temperatures, similar results for the detectability and degassing temperature were obtained by the SGP4x sensors (Figure 25). The initial degassing occurred at 112 °C with a delay up to 120 °C (a). The samples after 144 and 200 hours shift gradually to higher temperatures with an initial degassing at 115 °C (b) and 118 °C (c). The main response of the pixels stays at around 120 °C. The sample after 312 hours (d)

Klima- und Energiefonds des Bundes – Abwicklung durch die Österreichische Forschungsförderungsgesellschaft FFG

matches the initial degassing response of the unaged sample at 112 °C (a). This behavior was the same for the SGP30 sensors.

In terms of detectability a gradual decrease can be observed, although the lower detection limit is surpassed, ensuring a response of the sensors.

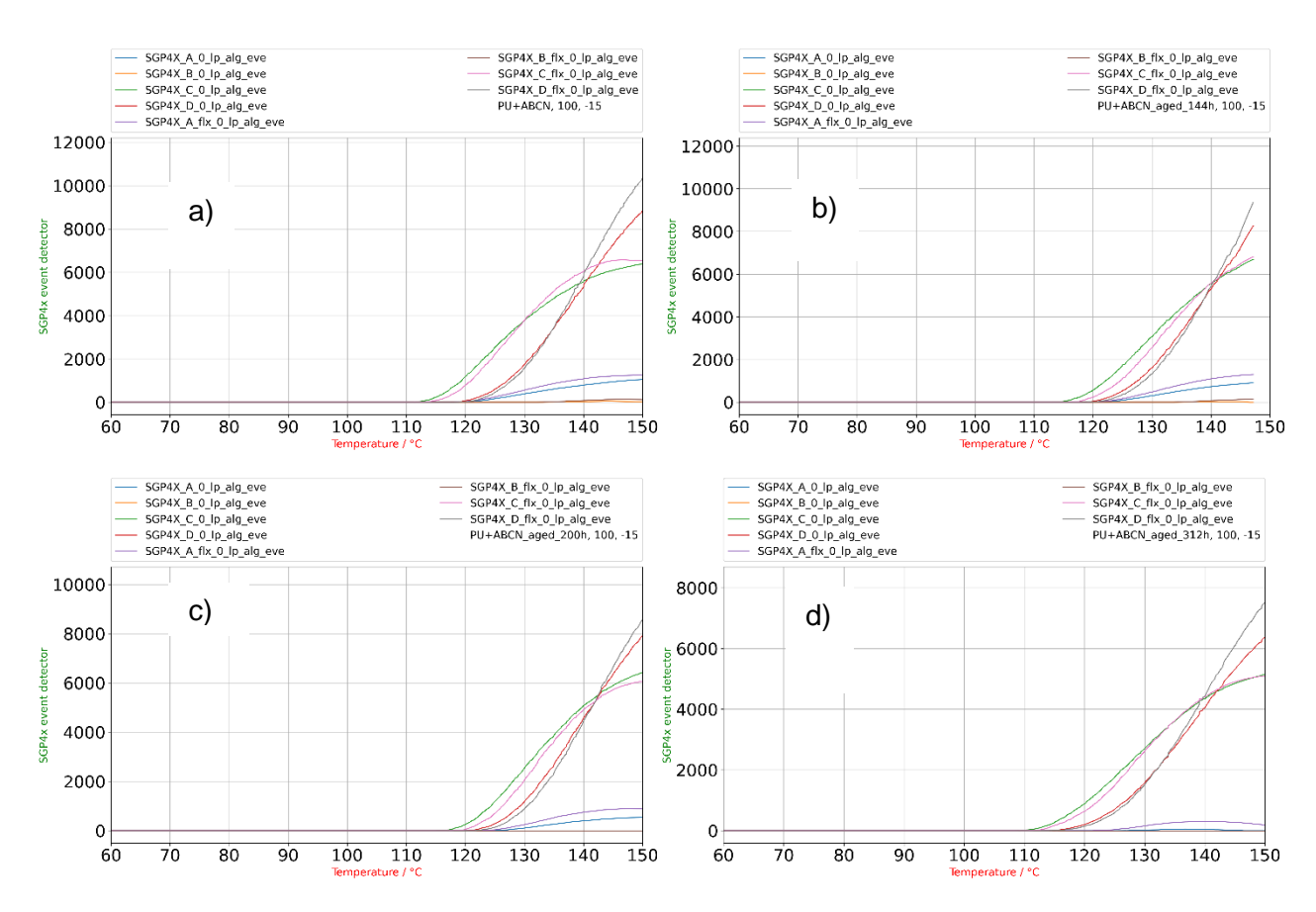


Figure 25: Comparison of detectability and degassing temperature of the ABCN additive by the SGP4x sensors over the course of a 312-hour aging test. Sample after 0 hours (a), after 144 hours (b), after 200 hours (c) and after 312 hours (d).

To extend the long-term stability measurements, samples were aged up to 84 days at different temperatures. The first experimental series kept the samples at room temperature for 84 days. Gradually at 21-, 42- and 84-days part of the samples were removed for closer examination. The degassing temperature was determined and compared for the different stages of ageing. Figure 26 shows the degassing temperature of the samples and additionally, a comparison of all three samples (d). The 21-day old sample shows a degassing temperature of 118°C (a), the 42-day old sample of 120°C (b) and the 84-day old sample of 119°C (c). The ageing did not increase the degassing temperature by much, indicating a rather good long-term stability at room temperature.

Klima- und Energiefonds des Bundes – Abwicklung durch die Österreichische Forschungsförderungsgesellschaft FFG SGP4X_A_0_lp_alg_eve SGP4X_B_0_lp_alg_eve SGP4X_C_0_lp_alg_eve SGP4X_D_0_lp_alg_eve SGP4X_A_fix_0_lp_alg_ev SGP4X_A_0_lp_alg_eve SGP4X_B_0_lp_alg_eve SGP4X_C_0_lp_alg_eve SGP4X_D_0_lp_alg_eve SGP4X_A_fix_0_lp_alg_eve SGP4X_B_flx_0_lp_alg_eve SGP4X_C_flx_0_lp_alg_eve SGP4X_D_flx_0_lp_alg_eve PU+ABCN_RT_42d, 100, -15 a) b) SGP4X_A_0_lp_alg_eve SGP4X_B_0_lp_alg_eve SGP4X_C_0_lp_alg_eve SGP4X_D_0_lp_alg_eve SGP4X_A_fix_0_lp_alg_eve SGP4X C 0 lp alg eve 21d - SGP4X C 0 lp alg eve 84d SGP4X_C_0_lp_alg_eve_42d d) c)

Figure 26: Comparison of detectability and degassing temperature of the ABCN additive by the SGP4x sensors over the course of an 84-day aging test at room temperature. Sample after 21 days (a), after 42 days (b), after 84 days (c). Comparison of all three samples with the best performing pixel of the sensor(d).

Another set of samples was aged for the same time at an elevated temperature of 40°C. The samples to be investigated were removed gradually after 21-, 42- and 84-days. Figure 27 summarizes the results of the single samples and additionally, shows a comparison of the different ageing states (d). This testing series shows no significant degassing temperature deviations with advancing ageing state. The sample after 21-days shows a degassing temperature of 119°C (a), after 42 days the temperature was at 115°C (b) and after 84 days the degassing temperature was recorded at 117°C (c).

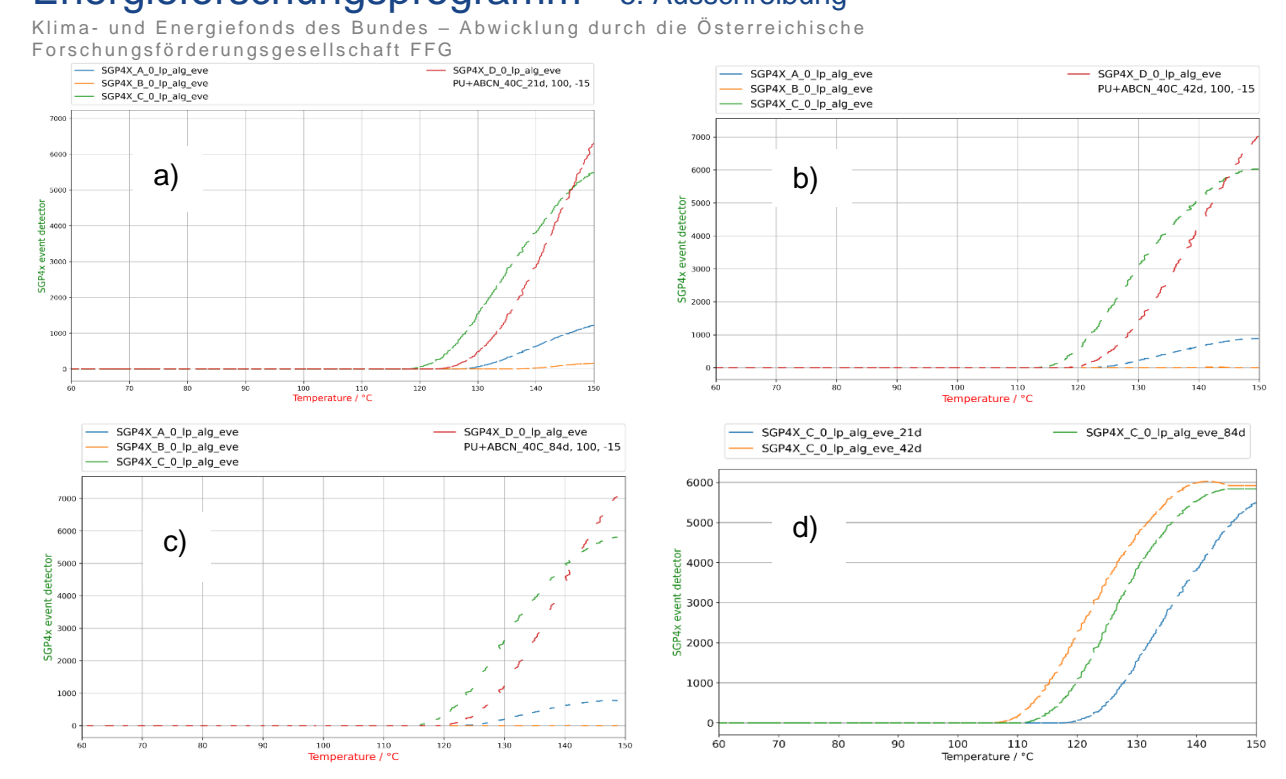


Figure 27: Comparison of detectability and degassing temperature of the ABCN additive by the SGP4x sensors over the course of an 84-day aging test at 40°C. Sample after 21 days (a), after 42 days (b), after 84 days (c). Comparison of all three samples with the best performing pixel of the sensor(d).

A third set of samples was tested for the same time at a temperature of 50°C. Part of the sample was removed from the testing chamber at the previously mentioned ageing states. Figure 28 shows the results of the investigation. A similar result as for the testing series at 40°C was obtained. The sample after 21 days has a degassing temperature of 118°C (a), after 42 days it shifted to 114°C (b) and after 84 days 117°C (c) were recorded.

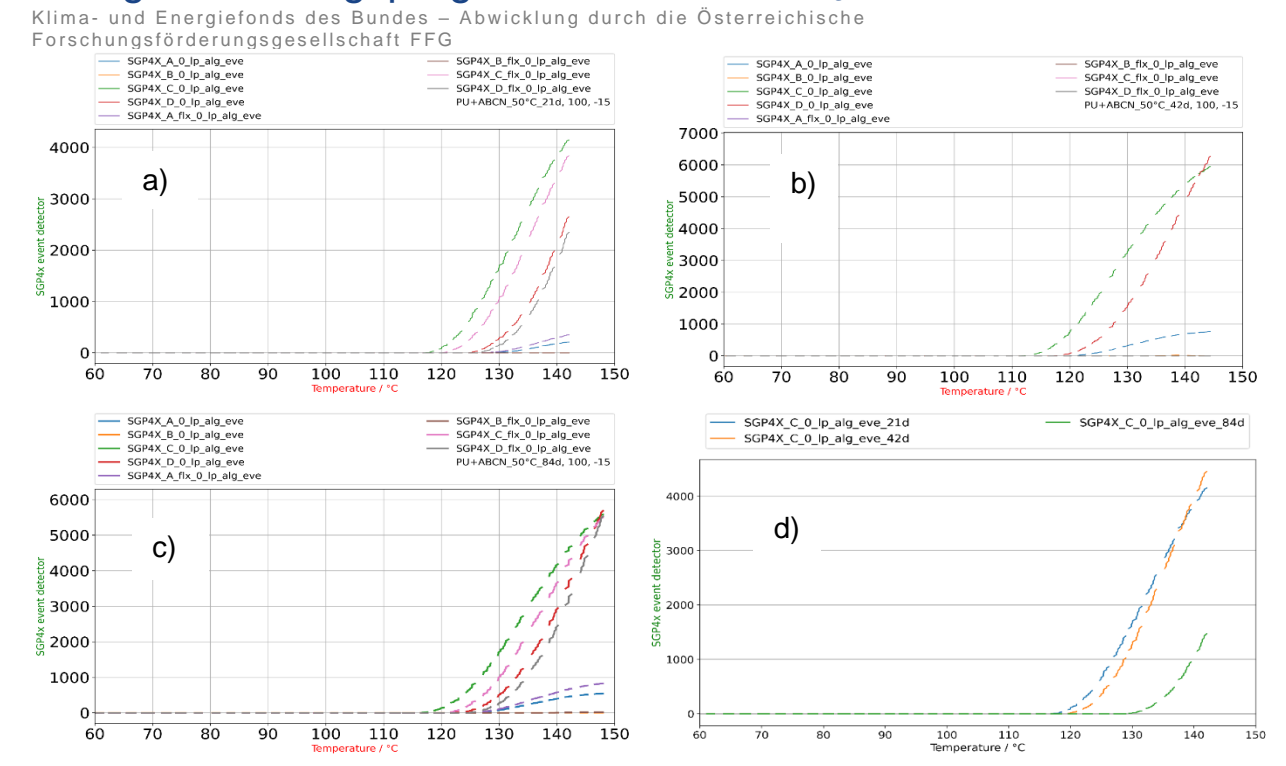


Figure 28: Comparison of detectability and degassing temperature of the ABCN additive by the SGP4x sensors over the course of an 84-day aging test at 50°C. Sample after 21 days (a), after 42 days (b), after 84 days (c). Comparison of all three samples with the best performing pixel on the sensor(d).

The last set of samples was tested at a temperature of 60°C for the same time as the previous mentioned. Parts of the sample were removed after certain time periods for a closer examination. Figure 29 shows the result of the test. The sample after 21 days has a degassing temperature of 118°C (a), after 42 days the temperature shifted to 120°C (b) and after 84 it shifted further to 130°C (c). The increase in degassing temperature indicates the occurrence of an ageing process, resulting in a later detection of the tracer gas. The deviation of temperature is likely a result of the discovery in D4.3, Results and discussion.

Klima- und Energiefonds des Bundes – Abwicklung durch die Österreichische Forschungsförderungsgesellschaft FFG

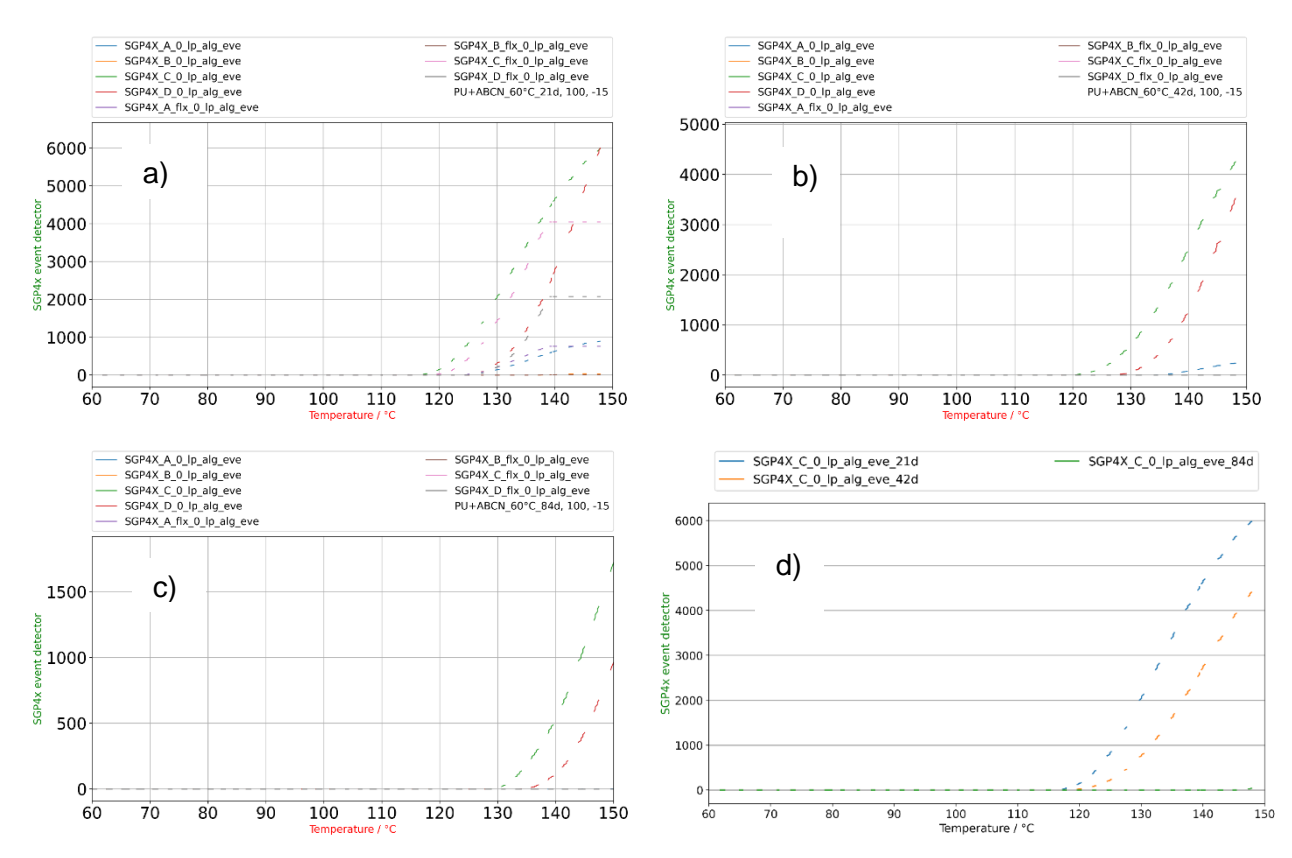


Figure 29: Comparison of detectability and degassing temperature of the ABCN additive by the SGP4x sensors over the course of an 84-day aging test at 60°C. Sample after 21 days (a), after 42 days (b), after 84 days (c). Comparison of all three samples with the best performing pixel of the sensor(d).

Aging effect of the AIBN additive

The AIBN samples were aged up to 312 hours together with the ABCN samples. The two main parameters to be determined are the release temperature and the detectability of the tracer gas.

A similar behavior for the degassing temperature and detectability can be seen for the SGP4x sensors (Figure 30). The unaged sample shows an initial degassing temperature at 109 °C and a second response at 115 °C (a). The rather early detection shifts to higher values after an aging time of 144 hours with a degassing temperature at 115 °C up to 118 °C (b). The sample aged for 200 hours has no meaningful sensor data recorded. After an aging time of 312 hours the degassing temperature shifted up to 119 °C (c).

Both sensors recorded a similar degassing behavior of the sample with the difference in the offset temperature for the SGP30 sensor. Regarding the detectability, the SGP4x shows a higher sensibility than the SGP30.

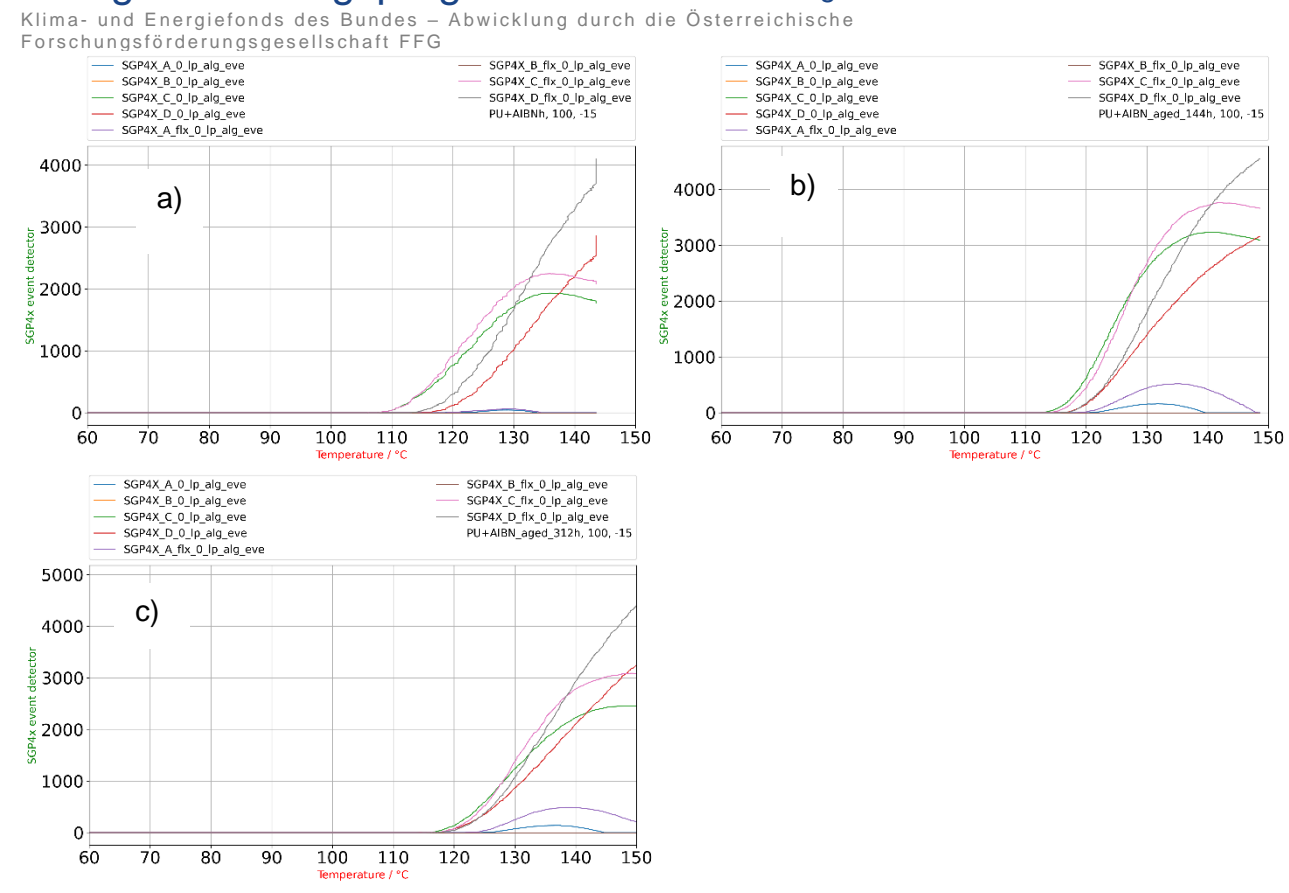


Figure 30: Comparison of detectability and degassing temperature of the AIBN additive by the SGP4x sensors over the course of a 312-hour aging test. Sample after 0 hours (a), after 144 hours (b) and after 312 hours (d).

Comparison of Gen 1.2 additives

Comparing the results of the ABCN and AIBN additive, ABCN shows a better long-term stability due to the smaller degassing temperature shifts. Those temperature changes occur due to the lower amount of additive in the matrix. Generally, the detectability declines over the course of time, especially the SGP30 due to the lower detection sensitivity.

We can conclude that AIBN has a promising early failure detection in terms of overtemperature for battery cells, but the long-term stability is poor. ABCN triggers a later sensor response in contrast to AIBN, but remains within the target temperature of 120 °C.

3.4.6 Diffusion in showcase

The advection experiments were expanded to a more realistic environment. Therefore, the battery pack replica was constructed. The experiments included electrolyte and tracer gas which was detected by SGP4x sensors. 1 mL of headspace of Leaf and EC/DMC (3/7) electrolyte was infused with a syringe. The detection times were measured in the enclosed battery pack replica. In a second step the experiments were repeated with ventilation in the pack.

Gen 1.2 samples were heated on a heating cell dummy, located in the middle of the showcase. The detection time of the released tracer gases were measured within the enclosed system.

Klima- und Energiefonds des Bundes – Abwicklung durch die Österreichische Forschungsförderungsgesellschaft FFG

Electrolyte diffusion

Two different electrolytes, Leaf and EC/DMC (3/7) were tested in the experimental series. Leaf was tested in the enclosed showcase without any ventilation (Figure 31). The injection of the electrolyte is clearly detected by the sensor positioned next to the inlet. The further away the sensors are positioned the more unpredictable the sensors detection is. Two third of the experiments show only one additional sensor, located in the middle of the showcase, which detects the electrolyte. In one third of the experiments, the electrolyte was detected by three sensors.

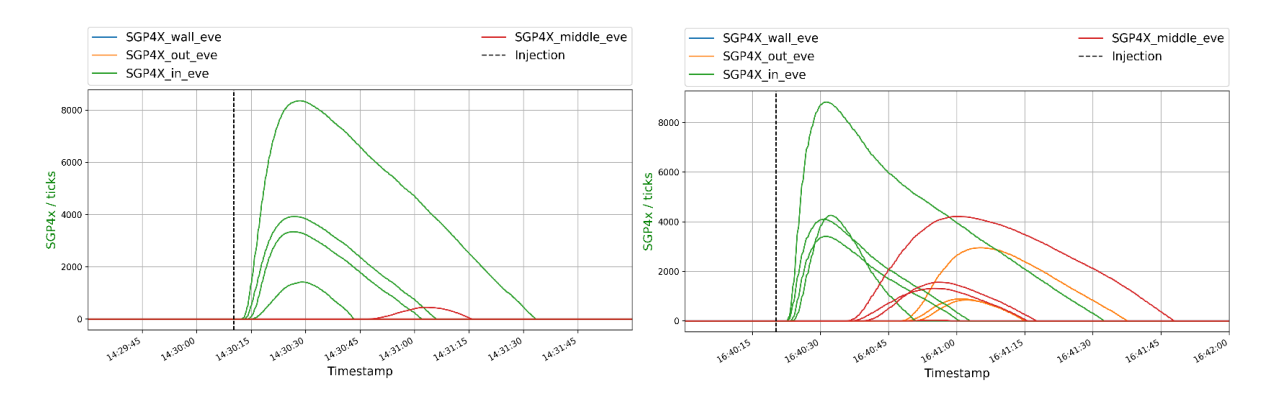


Figure 31: Leaf diffusion within an enclosed showcase setup. Injection of 1 mL headspace with a syringe.

The electrolyte EC/DMC was tested within an enclosed setup and a ventilated setup. 1 mL of headspace of the electrolyte was injected with a syringe in the enclosed setup for the first experiments (Figure 32). The electrolyte is registered immediately by the sensor positioned at the inlet of the showcase. Within 40s the sensor at the enclosed outlet of the battery pack replica detects the electrolyte as well. The sensor located in the middle of the showcase detects the electrolyte within 15s. Merely the sensor located on the wall diagonally opposite the injection point does not register the EC/DMC vapor.

Klima- und Energiefonds des Bundes – Abwicklung durch die Österreichische Forschungsförderungsgesellschaft FFG

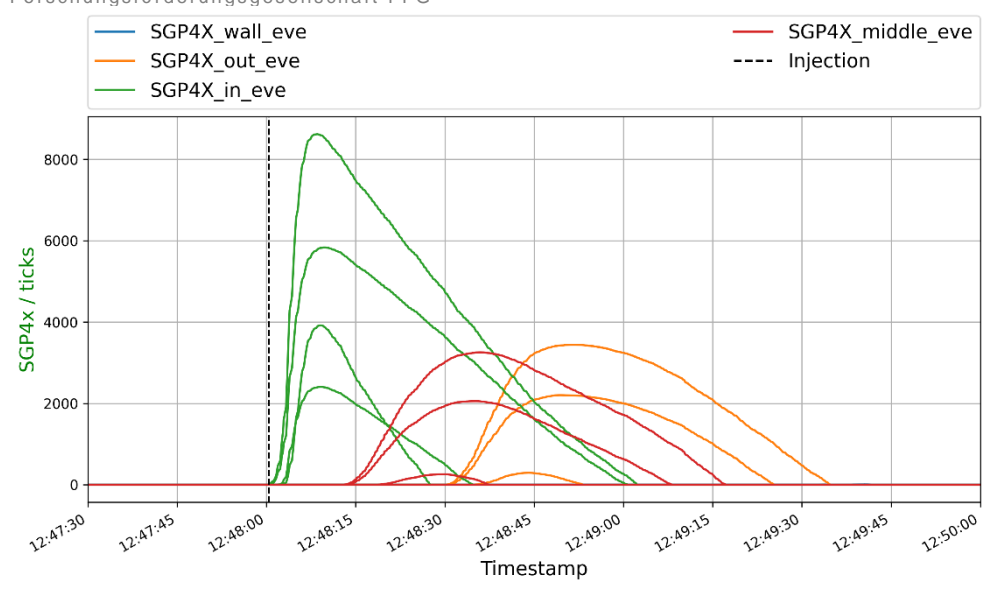


Figure 32: EC/DMC diffusion within an enclosed battery pack replica. 1 mL of headspace was injected with a syringe.

The good detectability of EC/DMC in the enclosed system was followed by experiments with different ventilation strengths within the showcase. The ventilation was achieved through an airflow at the gas inlet. The outlet on the diagonal opposite side of the showcase was opened to let the air escape. The flow of compressed air was controlled with a flow regulator. The airflow corresponded to 0.2 l/min, 0.5 l/min, 1 l/min and 2 l/min for every new experimental series respectively.

An airflow of 0.2 l/min did not improve the detectability of the electrolyte compared to the experiment in the enclosed system (Figure 33). The only sensor showing a detection signal was at the injection point. The increase to 0.5 l/min increased the sensor responses. Three sensors detected the electrolyte, at the injection point, the middle of the showcase and at the outlet. The last detection being at the outlet with a time delay of 60s after the injection. Increasing the airstream to 1 l/min did not change the sensor detectability but reduced the maximum detection time to 50s. A further increase of the airstream to 2 l/min reduced the detection time to 40s.

Klima- und Energiefonds des Bundes – Abwicklung durch die Österreichische Forschungsförderungsgesellschaft FFG

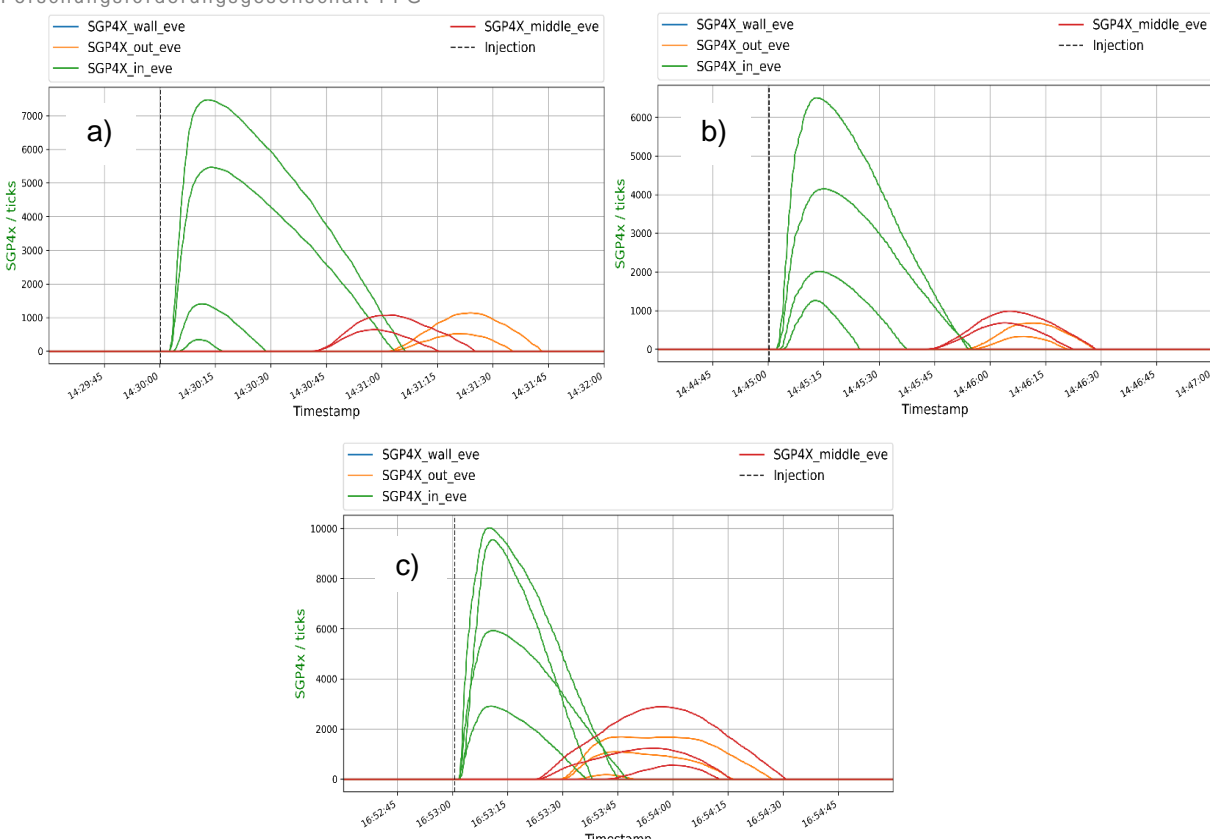


Figure 33: EC/DMC diffusion with airflows of compressed air of 0.5 l/min (a), 1 l/min (b) and 2 l/min (c).

Generation 1.2 samples

The battery pack replica was adapted with a heating possibility to evaluate the Gen 1.2 samples. A dummy cell with a heating pad on the inside was placed in the middle of the showcase. The sensor positions were not altered compared to the previous electrolyte diffusion experiments. The sample was placed on top of the dummy cell and heated to 140 °C. The experiments were conducted within the enclosed showcase without any ventilation.

The sample sizes were increased from 0.85 g until 1.6 g for the last experiment. The gradual increase in sample size was intended to render a minimal amount of sample necessary to be detected. The last experiment with 1.6 g sample shows a shift in sensor signal from the different sensor positions (Figure 34). But the signal change is not large enough to trigger an event from the algorithm.

Klima- und Energiefonds des Bundes – Abwicklung durch die Österreichische Forschungsförderungsgesellschaft FFG

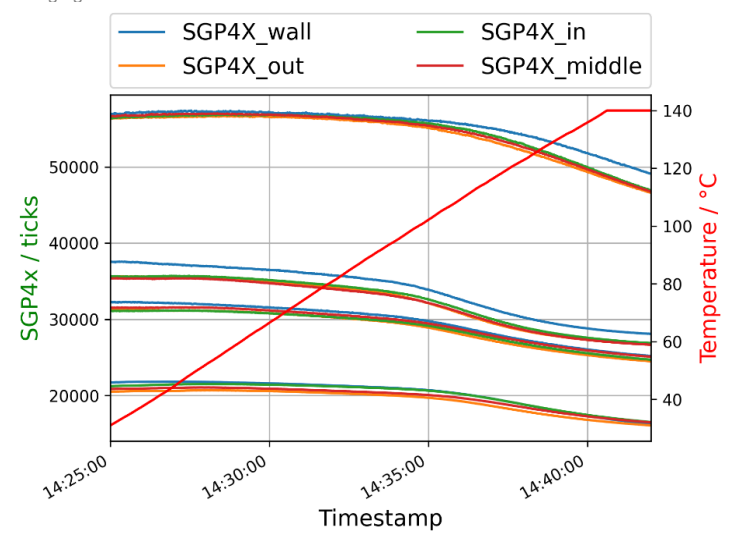


Figure 34: Raw sensor signals of the 1.6 g sample with pixels of four different sensor positions within the showcase. The pixels of one sensor are shown in the same color.

3.5 Validation of the sensors in battery systems.

In the first test cycle, started in August 2021, two sensor boxes from project partner UnraveITEC were placed in an EV-Battery-Pack. The sensor boxes contained different gas sensors from a variety of suppliers. The sensor boxes were placed inside the Battery-Pack at two locations which could resemble possible locations for BMS-Electronics. In addition to the two sensor boxes, there were five small ceramic heaters distributed in the Battery-Pack. The ceramic heaters were connected to functional polymer samples, provided by project partner PCCL, which was a mixture of PU and ABCN.

For each test, one of the ceramic heaters was activated to follow a specified temperature profile. The temperature profile started at 80°C and the temperature was increased every 30min by 10°C. The profile ended at 160°C. The temperature profile was controlled by an external Temperature controller unit. The sensor signals of all the gas sensors in both sensor boxes were recorded via CAN-Interface during each test.

Unfortunately, the SGP4x sensors had a suspicious rectangular modulation on its output signals, therefore it was not clear if these sensor-outputs were to be trusted. First examinations by SDIBS led to the assumption that the modulation frequency was somehow temperature-dependent, but in the end, this was not proven. It took some time and effort by project partner UnravelTEC to find, and fix, a bug in the firmware which caused this misbehaviour of the SGP4x.

After this bug was fixed, the tests had to be repeated und the measurements were analysed. The focus was put on the SGP4x sensor which was provided by project-partner SENSIRION. In previous test, conducted by project partners VIF and TU Graz, the SGP4x showed the most

Klima- und Energiefonds des Bundes – Abwicklung durch die Österreichische Forschungsförderungsgesellschaft FFG

Figure 36 sensor 2 is located closer to the polymer sample.

promising response to the outgassing of the PU+ABCN polymer. The test results show that the sensor which is located closer to the functional polymer has a more pronounced response than the one which is located farther away. This behaviour is seen in Figure 35: sensor 1 is located closer to the outgassing polymer, the stronger signal-response is clearly visible. In

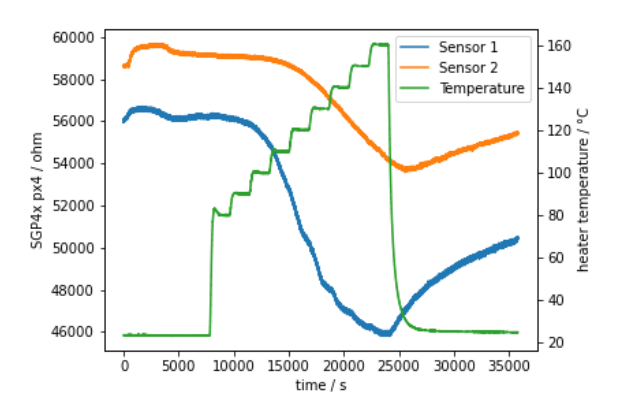


Figure 35: In this test, sensor 1 is located closer to the outgassing polymer, the stronger signal response is clearly visible.

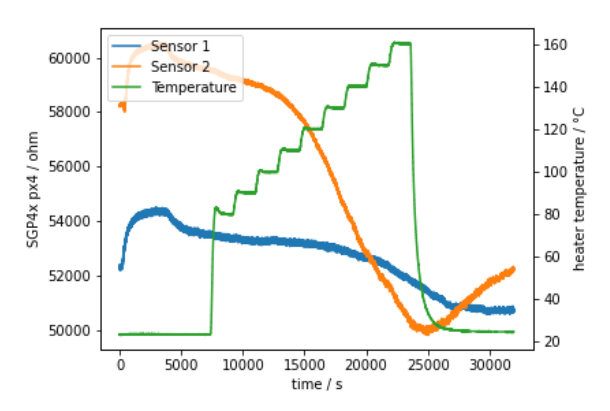


Figure 36: In this test, sensor 2 is located closer to the outgassing polymer, the stronger signal response is clearly visible.

The test results show that the signal amplitude gets stronger around 120°C which is the expected behaviour of the functional polymer. However, the response time seems to be quite slow, this can be due to the slow distribution of the gas inside the battery pack.

3.5.1 FUSA Concept

The high-level requirements for a gas-sensor system from view of functional safety were developed. It was evaluated at which general safety goals of a battery pack a gas sensor can have a physical interaction. Two safety functions are relevant for gas sensors and polymer coatings: "over temperature monitoring" and "thermal event detection".

Klima- und Energiefonds des Bundes – Abwicklung durch die Österreichische Forschungsförderungsgesellschaft FFG

3.6 Building of sensor platforms

3.6.1 ViF platform containing the following sensors was built:

The sensor platform is based on the "UnravelTEC Topping 1.0", using digital and analogue sensor interfaces. A Wifi interface is provided for live view of the data with a time delay of less than 3 seconds for digital and less than 0.3s for analogue sensors.

- Alphasense 4x: NO, NO₂, MOx VOC, PID VOC - analogue
- Figaro TGS5141 (CO) analogue
- AMS iAQ-Core (H₂, VOC) digital
- Sensirion SCD30 (CO₂, rH, T) digital
- Bosch BME280 (rH, T, P) digital
- SGX MiCS6815 (3x MOx) analogue
- IDT SGAS (H₂) analogue

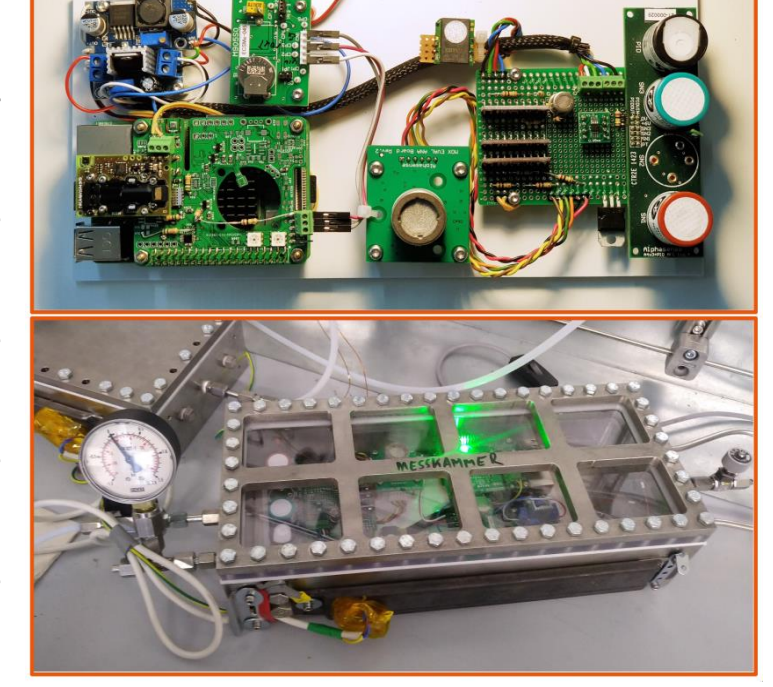


Figure 37: Top: Platform mounted on acryl base plate Bottom: Platform inserted into ViF *gas*-tight box

 4x ADS1115 ADCs for 12 singlechannels and 2 differential channels

All analogue sensors are read out via ADCs first which are connected to I2C to the host. For the Alphasense MOx and the SGAS, two low-noise voltage regulators were implemented to reduce sensor noise.

Klima- und Energiefonds des Bundes – Abwicklung durch die Österreichische Forschungsförderungsgesellschaft FFG

3.6.2 IES/TUG platform containing the following sensors

- Alphasense 2x: NO₂, NO analogue
- Sensirion SCD30 (CO₂, rH, T) digital
- Sensirion SGP30 (H₂, VOC) digital
- Bosch (rH, T, P) digital
- SPECsense (O₃/NH₂) digital



Figure 38: Platform for IES/TU Graz

3.6.3 Battery test system for Samsung SDI.

The systems use an embedded Linux computer to control the sensors, capture and store sensor data on an internal time series database. An especially compact system (Raspberry Pi Zero W) was used to connect the sensors and a CAN interface HAT. To accommodate the small size (20x80x60mm), a custom-designed 3D-printed enclosure was used (see Figure 4). A custom power supply for 12V was developed to provide a low-noise voltage, especially for the analogue sensors. Sensor data is sent live via CAN to the Samsung SDI battery test stand. The following sensors are included in the battery box:

- Sensirion SCD30: (CO₂, rH, T)
 digital
- Sensirion SGP30: (H₂, VOC) digital
- Figaro TGS5141: (CO), analogue
- AMS iAQ-Core (H₂, VOC) digital
- Bosch BME280 (rH, T, P) digital
- SGX MiCS6814 (3x MOx) analogue
- IDT SGAS (H₂) analogue
- 2x ADS1115 ADCs for 8 singlechannels





Figure 39: Battery Test box

Klima- und Energiefonds des Bundes – Abwicklung durch die Österreichische Forschungsförderungsgesellschaft FFG

3.6.4 Update of existing ViF platform

- Sensirion SGP4x prototype (4-channel MOx) digital
- Figaro TGS8100 (rH, T, P) analogue
- a fifth ADS1115 ADC (4 single-channel): 1 used for Figaro TGS8100, 3 free

All new sensors are stacked with an interface board on top of the existing sensor platform.

- For the SGP4x, a custom interface PCB with an 1.8V voltage regulator and level shifter was designed and equipped with fresh SGP4x sample chips from Sensirion.
- For the TGS8100, a fifth ADC was added to the interface board.

On the Software side, a new i2c sensor driver for the SGP4x was developed and integrated into the UnraveITEC data acquisition system. The TGS8100 is read out via the existing ADC drivers.

All new sensors were integrated into the frontend.

3.6.5 New microcontroller-based sensor platform for battery tests

For battery tests at Samsung SDI a completely new microcontroller-based platform (using an ATMEGA328) was developed with the following sensors (Figure 40):

- BME280 (rH, T, P)
- MiCS6814 (3 MOx channels, analogue)
- SGP30 (2 MOx channels read out)
- SGP4x (4 MOx channels)
- TGS5141 (1 electrochemical channel for CO, analogue)

The analogue sensors are read out via a 4-channel 16bit ADC (ADS1115). All analogue sensors (and the SGP4x) are read out with 10Hz, the others with 1Hz. Data is transmitted instantly via CAN-bus for live view by Samsung SDI, Therefore, no internal storage is needed. For debugging while mounted inside the battery, a serial port is integrated into the connection cable.

Klima- und Energiefonds des Bundes – Abwicklung durch die Österreichische Forschungsförderungsgesellschaft FFG

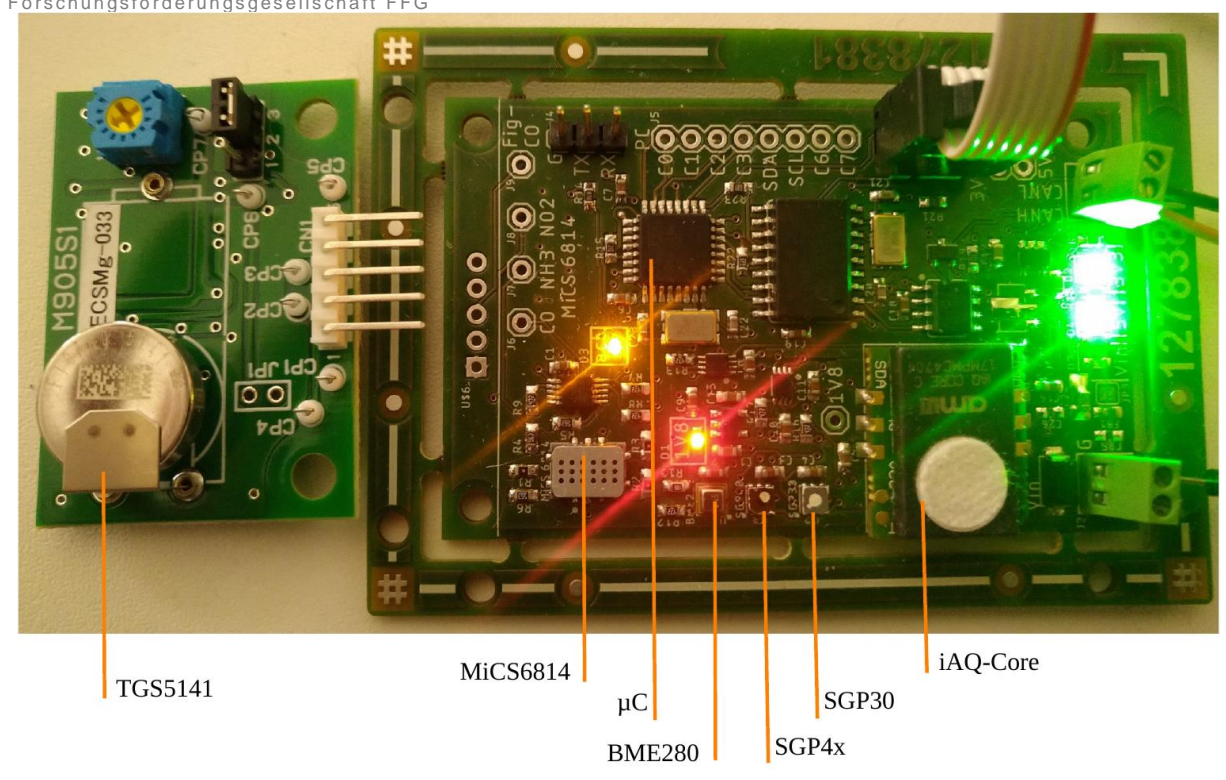


Figure 40: Microcontroller-bases sensor board for battery tests

At time of writing, one measurement box was passing the stability tests for one week flawlessly, the second is waiting for one sensor, whose delivery was postponed due to Covid-19. For the stability tests, a Raspberry Pi with CAN-Hat was used as a receiver. All sensor data are captured with 10 Hz in the Influx dabatase and can be visualized via Web-Frontend. The enclosure was 3D-printed. For choosing the material with the lowest probability of outgassing, four different materials were tested at ViF:

- ABS"NiceABS" (with better 3D-printing properties)
- PETG
- Polyamide

Due to the highest out-gassing temperature, PETG was chosen for the final enclosure (see Figure 41).

Klima- und Energiefonds des Bundes – Abwicklung durch die Österreichische Forschungsförderungsgesellschaft FFG



Figure 41: battery sensor platform, Gen2 with enclosure.

4 Results and conclusion

Sensor selection

To facilitate a relatively low-cost sensor platform and at the same time ensure proper detection of the additive (tracer gas) and precursor gases of battery failures, the decision was made to use mostly metal oxide (MOx) sensors. This sensor technology is based on the change of conductance (resistivity) upon the surface reaction with oxidizing or reducing gases. To obtain selectivity the sensors are typically coated with vendor specific materials. Cross-sensitivity to other gases is, however, always present.

Polymer development

The most suitable additives (ABCN and AIBN) were incorporated into a matrix based on polyurethane (PU). The thermal properties of this generation were carefully studied by thermo-analytical methods such as DSC, TGA and GC-MS, obtaining a high correlation between the various techniques. The additives thermally decompose in a temperature range from 100 – 120 °C. To complete the characterisation, ageing tests were performed to analyse the long-term stability of this generation. At moderate temperatures (25°C-50°C), the PU matrix containing ABCN showed a better long-term stability than the PU matrix containing AIBN, which showed a very fast decomposition rate, even at room temperature.

Sensor tuning

To overcome the generally low selectivity of individual MOx sensors it was decided to use a four-pixel MOx sensor platform which combines four separately controllable MOx sensors in a single package. In this way it was possible to configure some of the sensor pixels in such a way that the released target molecules show fingerprints for the investigated materials that are distinguishable from the fingerprints of various background compounds or competing gases that could occur in real use-case applications.

Klima- und Energiefonds des Bundes – Abwicklung durch die Österreichische Forschungsförderungsgesellschaft FFG

Finally, the data processing step is necessary to evaluate the recorded raw data such as to achieve an early warning signal indicating the upcoming of a critical battery state.

Validation in a battery system

The concept of the early failure detection was tested in a laboratory scale battery pack module replica and in a real battery pack system. The battery pack module was equipped with four SGP4x sensors and a polymer on top of a heating dummy cell. In the battery pack two sensor boxes were placed at two different locations, resembling possible locations for BMSelectronics. Five ceramic heaters with functional polymer samples were distributed throughout the battery pack.

The tracer gas from the polymers is detected by the sensors at around 120 °C. The samples located closest to the sensors trigger a more pronounced response.

The tests prove the concept of failure monitoring technology with low-cost gas sensors.

5 Outlook and recommendations

The prototype setup achieved during this project can now enter the field-testing phase as is realized through Samsung SDI as the main industrial project partner who can implement the system into its future products. Further cooperation towards a product inside battery cells is possible as far as it is compatible with the industrial partner's development plans.

The use of gas detection could be applied in battery charging and for other approaches, as an early failure mechanism, or for the detection of electrolyte or hydrogen. In this regard the use of polymers combined with additives seems useful, especially because polymers can be easily applied on various surfaces. The application can be expanded to areas other than the automotive industry.

Publication of the system including sensor technology and data processing concepts has been initiated in order to facilitate other research and/or development parties to improve the safety of battery systems.

Energieforschungsprogramm - 5. Ausschreibung Klima- und Energiefonds des Bundes - Abwicklung durch die Österreichische Forschungsförderungsgesellschaft FFG

Contact data

Project Lead: Christiane Essl Virtual Vehicle Research GmbH Inffeldgasse 21/a 8010 Graz +43 316 873 9001 info@v2c2.at

The project partners are:

TU-Graz: Technical University of Graz, Institute of Electrical Measurement and Sensor

Systems

Sensirion: Sensirion AG represented by Sensirion Automotive Solutions AG

PCCL: Polymer Competence Center Leoben GmbH

SDIBS: Samsung SDI Battery Systems GmbH

UnraveITEC: UnraveITEC